

## 4 Stable, static Curvature-cosmology

5 DAVID F.CRAWFORD<sup>1</sup>

6 <sup>1</sup>*School of Physics (Retired), University of Sydney, NSW, 2006, Australia*

7 (Dated: July 26, 2022)

### 8 ABSTRACT

9 This paper describes Curvature-cosmology that is a tired-light cosmology that predicts a well-defined  
10 static and stable universe. It provides a new simpler raw data analysis for Type Ia supernova. Since  
11 it is a complete challenge to the big bang paradigm, Curvature-cosmology can only be judged by  
12 its agreement with direct cosmological observations. Curvature-cosmology predicts a universe of a  
13 hydrogen plasma with a temperature of  $2.456 \times 10^9$  K [observed:  $2.62 \times 10^9$  K] and a cosmic background  
14 radiation temperature of 2.736 K [observed: 2.725K]. It has only one parameter which is the density  
15 of the cosmic plasma. The major observations that are shown to consistent with it are: Type Ia  
16 supernova, Tolman surface brightness, angular size, galaxy distributions, X-ray background radiation,  
17 and quasar variability. It does not need inflation, dark matter or dark energy.

18 *Keywords:* cosmology, supernova

19	Contents	40	4. Part C: Observations	15
20	1. Introduction	2	4.1. Type Ia supernova	15
21	2. Part A: Analysis of Type Ia Supernova	2	4.2. X-ray background radiation	15
22	2.1. Introduction	2	4.3. Cosmic microwave background radiation.	18
23	2.2. Type Ia supernova	3	4.4. Tolman surface .	18
24	2.3. The observations.	4	4.5. Dark matter and Coma cluster	20
25	2.4. Results for the light curve width	4	4.6. Angular size	22
26	2.5. Supernova absolute magnitudes.	6	4.7. Galaxy distribution	23
27	2.6. Discussion of SALT2 supernova	7	4.8. Quasar variability in time	24
28	magnitudes.	7	4.9. The Butcher-Oemler effect	24
29	3. Part B: Curvature-cosmology theory.	7	4.10. Fluctuations in the CMBR	25
30	3.1. Introduction	7	4.11. Pioneer 10 acceleration.	25
31	3.2. Derivation of Curvature-redshift	7	4.12. The Sunyaev–Zel’dovich effect	26
32	3.3. Gravitation is not a force	9	4.13. Gravitational lensing.	27
33	3.4. Derivation of Curvature-pressure.	10	4.14. Lyman_alpha forest	27
34	3.5. The Curvature-cosmological model	11	4.15. Nuclear abundances	28
35	3.6. Distance modulus.	12	4.16. Galactic rotation curves	28
36	3.7. Temperature of the cosmic plasma	12	4.17. Redshifts in our Galaxy	29
37	3.8. Black holes and Jets	13	4.18. Anomalous redshifts	29
38	3.9. Inhibition of Curvature-redshift	13	4.19. Voids	30
39	3.10. Possible laboratory tests.	14	4.20. Entropy	31
			4.21. Olber’s Paradox	31
			4.22. Philip’s relation	32
		63	5. Conclusions	32
		64	6. Author biography	33

## 1. INTRODUCTION

Nearby Type Ia supernovae are well known to have essentially identical light curves that make excellent cosmological probes. The observational evidence for their time dilation has a long history with notable papers being by Goldhaber et al. (2001, 1996); Blondin et al. (2008). More recent contributions are by Kowalski et al. (2008); Wood-Vasey et al. (2008); Kessler et al. (2009a); Amanullah et al. (2010); Conley et al. (2011); Betoule et al. (2014); Scolnic et al. (2018). All of these recent papers use the SALT2 Guy et al. (2010, 2007) method to determine the widths and peak flux densities of the supernova and they have used the  $\Lambda$ CDM expansion cosmology to determine absolute magnitudes.

These papers show that type Ia supernova observations provide the major contribution to cosmological models.

A crucial property of Curvature-cosmology is that the observed magnitude is the sum of an intrinsic magnitude, which is what would be observed by a nearby observer and a cosmological magnitude. The cosmological magnitude is a comes from the change in the average energy of the photons due to their trajectory through the universe. Whereas the intrinsic magnitude is only a property of the observed object and is completely independent of the cosmology.

This paper has three major parts where the first part presents a new much simpler method that analyzes raw Type Ia supernova data in order to produce their light curve widths and their peak flux densities. These results are compared with the standard SALT2 method and it showed that the SALT2 method (summarized in the appendix) has a flaw in its flux density results.

The second part presents a new static cosmology, Curvature-cosmology, that has excellent agreement with observations.

The third part provides the observation data for all major cosmological observations and discusses the results in the context of Curvature-cosmology.

It is followed in section 5 by a summary of the quantitative observations that are relevant to Curvature-cosmology.

The common attribute of all  $\Lambda$ CDM , cosmologies is that they are based on the assumption that the universe is expanding (Peebles 1993). An early alternative was the steady-state theory of Hoyle, Bondi and Gold Hoyle (1962) (described with later extensions by Hoyle et al. (2000)) that required continuous creation of matter. However steady-state theories have serious difficulties in explaining the cosmic microwave background radiation. This left  $\Lambda$ CDM as the dominant cosmology but still subject to criticism.

Lal (2010) and Joseph (2010) have continued major earlier criticisms of  $\Lambda$ CDM cosmologies (Ellis 1984; Lerner 1991; Disney 2000; van Flandern 1991). Whereas most of these criticisms have been of a theoretical nature, this paper concentrates on whether observational data supports a static cosmological model, Curvature-cosmology, described below.

The purpose of this paper is to examine all major cosmological observations and to show that with minor exceptions they are in agreement with a this static model.

This paper is the culmination of many years of work and is a complete re-synthesis of many approaches that I have already published (Crawford 1987a,b, 1991, 1993, 1995a,b, 1998, 1999a,b, 2006, 2009a,b). These papers are cited to show the convoluted and historical path of Curvature-cosmology. Because hypotheses and notations have changed and evolved, direct references to these earlier versions of the theory would be misleading and all relevant results are published in this paper.

For convenience it is assumed that the wavelength dependence of a band can be replaced by a single value,  $\lambda$ , which is the mean wavelength for that band.

## 2. PART A: ANALYSIS OF TYPE IA SUPERNOVA

## 2.1. Introduction

This part describes a new analysis method (intrinsic analysis) for Type Ia supernova that is simple and can replace the standard SALT2 method. A major difference from SALT2 is that it explicitly estimates and uses intrinsic flux densities. Its use in an analysis of 1,707 light curves for Type Ia supernova provides a width regression,

$$w_{obs}(z) = 1.060 \pm 0.009 + (1.080 \pm 0.042)z, \quad (1)$$

which is in excellent agreement with a  $(1+z)$  dependence and justifies the analysis method. An analysis of 635,218 quasar observations shows that their flux density is proportional to  $-(1+z)(1.0073 \pm 0.0046)$  which verifies a universal energy  $(1+z)$  dependence.

It is shown that absolute magnitudes of Type Ia supernova analyzed with the SALT2 method and using the  $\Lambda$ CDM distance modulus are independent of redshift. However supernova analyzed with the intrinsic analysis and using the  $\Lambda$ CDM distance modulus have a significant dependence on redshift which implies a fault in the SALT2 analysis .

Although the intrinsic magnitude is the same as apparent magnitude, the different name is used because the measurement method is different. The intrinsic magnitude can only be used when there are many bands and relies on the fact that each **band** must have the same

165 cosmological magnitude. Whereas the apparent magni-  
166 tude can be applied to a single observation.

167 The next section covers the results for intrinsic magni-  
168 tudes for both Type Ia supernova and quasars. An im-  
169 portant product is plots of intrinsic magnitudes verses  
170 intrinsic wavelengths, both of which appear to be domi-  
171 nated by atomic hydrogen absorption.

172 Section 2.5 is about absolute magnitudes. Although  
173 the absolute magnitudes for supernova analyzed with  
174 the SALT2 method and the  $\lambda$ CDM model show no de-  
175 pendence with redshift. The absolute magnitudes for  
176 intrinsic analysis and the  $\lambda$ CDM model are significantly  
177 different from zero

178 Section 2.6 Provides a discussion of why the  $\lambda$ CDM  
179 model may be flawed.

## 2.2. Type Ia supernova

180  
181 From Wikipedia: “Type Ia Supernova is believed to  
182 result from mass accretion to a carbon-oxygen white  
183 dwarf in a close binary system. When the white dwarf  
184 mass exceeds the Chandrasekhar limit, the degenerate  
185 electron pressure can no longer support the accumulated  
186 mass and the star collapses in a thermonuclear explosion  
187 producing a supernova. The peak luminosity of super-  
188 nova Ia is set by the radioactive decay chain, and the  
189 observed photometric correlation between the peak lu-  
190 minosity and the time-scale over which the light curve  
191 decays from its maximum is understood physically as  
192 having both the luminosity and opacity being set by the  
193 mass of Nickel-56 synthesized in the explosion.”

194 The major observational evidence for Type Ia super-  
195 nova is a lack of hydrogen lines and a singly ionized  
196 silicon (Si II) absorption feature at  $0.615\mu\text{m}$  near peak  
197 brightness.

198 The observation of a distant supernova requires the  
199 emission of a photon from an intrinsic source and then it  
200 follows a trajectory that is determined by the geometry  
201 of the universe. If the universe is expanding then their  
202 average energy is determined by velocity of the telescope  
203 relative to the source. If the universe is static, this en-  
204 ergy loss could be the result of photons being scattered  
205 outside the beam.

206 A critical part in measuring the light curve width of  
207 Type Ia supernova light curves is to have a reference  
208 light curve. The observed light curve must have the  
209 same shape independent of redshift. Only its width and  
210 height will vary with redshift. Consequently this prop-  
211 erty is assumed in intrinsic analysis.

212 In order to remove any possible bias, a standard in-  
213 dependent template, the *B* band Parab-18 from Table 2  
214 from Goldhaber et al. (2001) which has the first half-  
215 peak width at -10.1 days and the second half-peak width

216 at 22.3 days is used. Consequently all widths are relative  
217 to this light curve.

218 The purpose of the light-curve analysis is to obtain  
219 estimates of the peak flux density for each band, the  
220 width (common to all bands) of the light-curve relative  
221 to the template and the epoch offset of the light curve.  
222 This offset is a nuisance parameter that allows for the  
223 unknown epoch of the peak flux density and is defined  
224 to be the epoch difference between the fitted light curve  
225 relative to the observed epochs.

226 An initial problem is to determine the initial epoch  
227 offset  $q$ . The solution used was to estimate the aver-  
228 age flux density for every epoch in the observed range.  
229 This averaging used a Gaussian weight factor with the  
230  $weight = \exp(-0.5(p_i - q)^2)$  where  $p_i$  is the epoch of an  
231 observation and  $q$  is the reference epoch. The day with  
232 the largest average flux density defined the initial epoch  
233 offset.

234 The intrinsic analysis method starts with the observed  
235 flux density,  $f_i$  for the index  $i$ , and its uncertainty  $\sigma_i$ .  
236 Then for each supernova and each band the maximum  
237 likelihood method is used to determine the fitted maxi-  
238 mum flux density,  $F$  and its epoch.

239 Let the reference supernova light curve be referenced  
240 by  $C((p_i - q)/w)$  where  $p_i$  is the epoch,  $w$  is the com-  
241 puted width, and  $q$  is the epoch offset of the maximum  
242 of the fitted light curve. Then, assuming a Gaussian flux  
243 density noise distribution, the log-likelihood function for  
244 a single band, with  $n$  observations, of a supernova is

$$\mathcal{L} = \sum_{i=1}^n \left[ \left( \frac{f_i - b - F \times C((p_i - q)/w)}{\sigma_i} \right)^2 \right] \quad (2)$$

245 where  $i$  is the observation index, the epoch is  $p_i$  and  $b$   
246 is the base flux density level for the current band. A  
247 constant term that depends only on the measurement  
248 uncertainties is omitted. Additionally the omission of  
249 the factor  $-1/2$  means that  $\mathcal{L}$  is a  $\psi^2$  variate with  $n$   
250 degrees of freedom. Thus the maximization of the like-  
251 lihood is identical to the minimization of  $\mathcal{L}$ .

252 Although the peak flux density and base level are de-  
253 termined by an analytic fit, the values for the epoch  
254 offset and width are easily found by numerical mini-  
255 mization. Fortunately, the flux density and width are  
256 almost orthogonal so that a sequence of alternate fits  
257 rapidly converges.

258 Note that in Eq 2 each flux density and each peak  
259 flux density is divided by its uncertainty which means  
260 that the fitted width is independent of individual band  
261 calibrations and all bands can be included in the same  
262 expression.

263 All the information about the width distribution is  
264 contained in  $\mathcal{L}$ . The uncertainty in the width was deter-

265 mined from the proposition that the likelihood function,  
 266  $\mathcal{L}$  as a function of width is equal to the likelihood of a  
 267 Gaussian function of width with a standard deviation  
 268 equal to the width uncertainty. That is

$$\mathcal{L} = \left(\frac{\Delta w}{\sigma_w}\right)^2, \quad (3)$$

269 where  $\Delta w$  is the width offset and  $\sigma_w$  is the estimated  
 270 uncertainty in the width and it is estimated using Eq. 2.

271 It must be noted that the fitting procedure is com-  
 272 pletely independent of the redshift and is also indepen-  
 273 dent of the band type. Although each band had its own  
 274 estimate of its peak flux density, the width is the result  
 275 of a common fit to all observations for each supernova.  
 276 Thus the computed parameters for each supernova are  
 277 its light curve width, and the peak flux density for each  
 278 band which is the flux density for that band at the max-  
 279 imum epoch of the common fitted light curve.

### 2.3. The observations.

281 The Type Ia supernova data used here comes from  
 282 the Supernova Legacy survey (SNSL), the Sloan Digital  
 283 Survey (SDSS) (both sourced from the SNANA website  
 284 Kessler et al. (2009b)), and the Panoramic Survey Tele-  
 285 scope and Rapid Response System, (Pan-STARRS), su-  
 286 pernova survey Kaiser et al. (2010); Jones et al. (2018);  
 287 Scolnic et al. (2018) and those observed by the Hubble  
 288 Space Telescope (HST) Riess et al. (2007); Jones et al.  
 289 (2013).

290 The observations of Type Ia supernova from Pan-  
 291 STARRS, (PS1), were accessed from the site <https://archive.stsci.edu/prepds/ps1cosmo/jones>  
 292 //archive.stsci.edu/prepds/ps1cosmo/jones and the file  
 293 datatable.html. In 2018 Pan-STARRS consisted of two  
 294 1.8-m Ritchey-Chrétien telescopes located at Haleakala  
 295 in Hawaii and could record almost 1.4 billion pixels per  
 296 image. It is designed to detect moving or variable ob-  
 297 jects on a continual basis. An image with a 30 to 60  
 298 second duration can record down to an apparent magni-  
 299 tude of 22 mag. The whole visible sky will be surveyed  
 300 four times a month.

301 Although theoretically, the Type Ia supernova model  
 302 has a fixed absolute magnitude, its measurement is sub-  
 303 ject to the usual uncertainties. This is why they can be  
 304 observed at redshifts beyond the nominal limit of the  
 305 telescope and are subject to Malmquist bias.

306 However many of the observations come from the PS1  
 307 survey which is essentially providing a continuous record  
 308 of the sky so that the simple Malmquist bias is not appli-  
 309 cable. However for all the other supernova a Malmquist  
 310 bias of  $-1.382\sigma_i^2$  mag, where  $\sigma_i$  is the observed flux  
 311 density uncertainty was applied. (The application of  
 312 Malmquist bias corrections made negligible difference to  
 313 the results.)

**Table 1.** Light-curve numbers for each band

Band	$\lambda/\mu\text{m}$	$N^a$	$N^b$
U	0.365	77	0
B	0.445	121	0
V	0.551	121	0
R	0.658	72	0
I	0.809	74	0
u	0.354	141	0
g	0.475	421	1141
r	0.622	468	1132
i	0.763	468	1142
z	0.905	412	1146
F775W	0.771	7	0
F850LP	0.907	17	0

<sup>a</sup> Number of supernova from other catalogues.

<sup>b</sup> Number of supernova for the PS1 catalogue.

314 Table 1 shows the statistics for the selected supernova.  
 315 The selection criteria was that there was a good fit and  
 316 the width was between 0.3 and 5.0 and the width uncer-  
 317 tainly was less than 0.3. In addition the value of  $\mathcal{L}$  had  
 318 to be less than  $20/n$ .

### 2.4. Results for the light curve width

319 from 1,745 initial candidates there were 1,707 that  
 320 satisfied selection criteria. Most of the rejections were  
 321 because there were insufficient observations prior to the  
 322 peak epoch.

323 The important result of this width analysis is a re-  
 324 gression of  $w_{obs}(z)$  as a function of  $z$  for all the 1,707  
 325 accepted observations which is

$$w_{obs}(z) = (1.060 \pm 0.009 + (1.080 \pm 0.042))z. \quad (4)$$

326 Although the ordinate is statistically different from  
 327 one, it is this ordinate that is most sensitive to calibra-  
 328 tion and systematic errors such as having minor errors  
 329 in the reference light curve. Here this difference is not  
 330 important. However the coordinate shows an excellent  
 331 agreement with one. Note that this width is indepen-  
 332 dent any cosmological model.

333 The widths for all the supernova are shown in Figure 1.  
 334 It is clear that the slope is consistent with the expected  
 335 dependence of  $w(z) = 1+z$ . Some of the supernova show  
 336 either discrepant widths or discrepant uncertainties and  
 337 to avoid any bias, no rejections have been made to the  
 338 original data.

339 For convenience it helps to convert all the flux den-  
 340 sities into magnitudes. All computed apparent magni-  
 341 tudes except the those in the SDSS catalogue were cal-  
 342 culated by  $m_k = 27.5 - 2.5 \log_{10}(F_k)$  where  $F_k$  is the  
 343  
 344  
 345

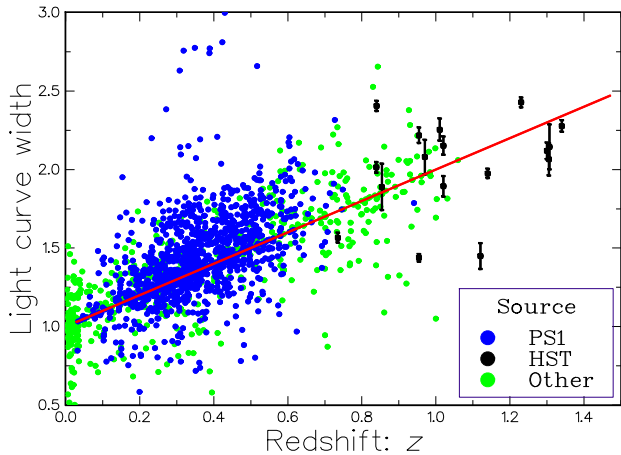


**Figure 1.** A plot of the Type Ia supernova light curve observed widths. The blue dots are for the PS1 and the black dots with error bars show the HST (Hubble Space Telescope) observations. All other observations are shown by the green dots. The red line shows a  $(1 + z)$  dependence

346 peak flux density and  $k$  is the band. Those in the SDSS  
347 catalogue had  $m_k = 24.5 - 2.5 \log_{10}(F_k)$ .

348 Since each supernova has a peak flux density for each  
349 observed band, they can be combined to provide a peak  
350 intrinsic flux density for each band and a cosmological  
351 flux density for the supernova. Thus there is a clear  
352 separation between the intrinsic flux density which is  
353 independent of the redshift and the cosmological redshift  
354 that is only a function of redshift.

355 Then for each supernova and band the fitted apparent  
356 magnitude is the sum of an intrinsic magnitude and a  
357 common cosmological magnitude. Starting with a constant  
358 intrinsic flux density, the average magnitude was  
359 determined by fitting a regression equation to the observed  
360 peak magnitudes minus the current intrinsic magnitude which  
361 is common to all the supernova and is a function of the  
362 intrinsic wavelength.

363 The first step is to estimate an initial cosmological flux  
364 density as the mean of the observed peak flux densities  
365 for each band. The next step is to determine an estimate  
366 of the intrinsic flux density as a function of the intrinsic  
367 wavelength,  $\psi$  which by definition is

$$\psi = \lambda / (1 + z). \quad (5)$$

368 Initially there 30 boxes that cover the  $\psi$  range are set to  
369 zero, then the difference between each observed flux density  
370 and the current estimate of the absolute magnitude  
371 is added to the appropriate box. After all the observations  
372 are processed, the procedure is repeated with each  
373 peak flux density being corrected for the average flux  
374 density defined by the mean of its box. Then a new  
375 set of cosmological magnitudes are produced. This pro-

376 cess is repeated until there are legible changes in all the  
377 values.

378 Thus each supernova has a peak cosmological magni-  
379 tude and there is a common intrinsic magnitude distri-  
380 bution. The individual intrinsic peak magnitude data  
381 points for the supernova are shown in Figure 2 and tab-  
382 ulated in Table 2. There is a very rapid decrease in  
383 the intrinsic luminosity as the intrinsic wavelength ap-  
384 proaches the Lyman $_{\alpha}$  line which suggests scattering in  
385 a local hydrogen cloud. This could also explain the lack  
386 of hydrogen lines in the spectra. Note that the size of  
387 this cloud would be very small and would not be easily  
388 detected.

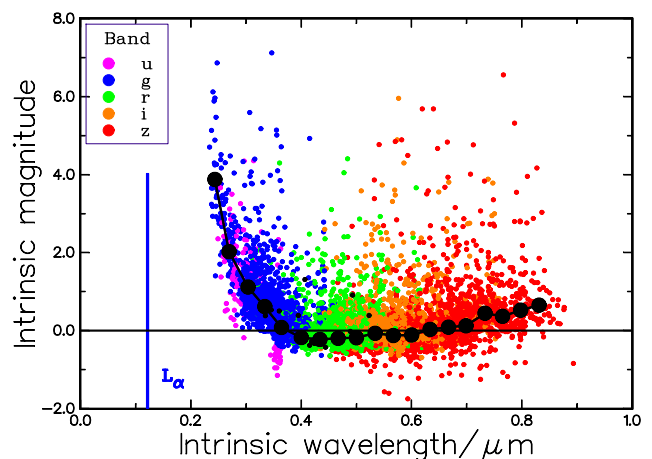


**Figure 2.** The intrinsic peak magnitude of Type Ia supernova as a function of intrinsic wavelength,  $\psi$ . The black points and curve show the average intrinsic peak magnitude as a function of intrinsic wavelength. The bands  $UBVRI$  have the same sequential colors as the bands  $ugriz$ . The position of the Lyman $_{\alpha}$  line is shown in blue.

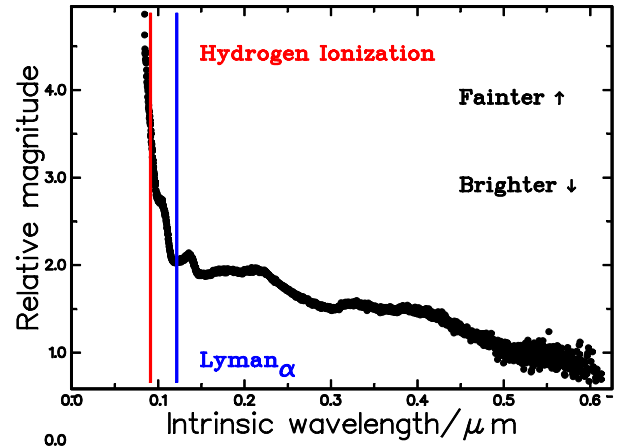
389  
390  
391 The purpose of this section is to show that an analysis  
392 of the observed magnitudes for many quasars is to show  
393 that they all have a relative energy loss of  $(1 + z)$ .

394 From Wikipedia: “A quasar also known as a quasi-  
395 stellar object is an extremely luminous active galactic  
396 nucleus (AGN), powered by a supermassive black hole,  
397 with mass ranging from millions to tens of billions times  
398 the mass of the Sun, surrounded by a gaseous accre-  
399 tion disc. Gas in the disc falling towards the black hole  
400 heats up because of friction and releases energy in the  
401 form of electromagnetic radiation. The radiant energy  
402 of quasars is enormous; the most powerful quasars have  
403 luminosities thousands of times greater than a galaxy  
404 such as the Milky Way. Usually, quasars are categorized  
405 as a subclass of the more general category of AGN. The  
406 redshifts of quasars are of cosmological origin.”



**Table 2.** Intrinsic magnitude of Type Ia supernova

box	number	$\psi/\mu\text{m}$	magnitude
8	26	0.243	$3.876 \pm 0.247$
9	132	0.269	$2.021 \pm 0.077$
10	256	0.304	$1.113 \pm 0.051$
11	471	0.334	$0.613 \pm 0.032$
12	608	0.364	$0.080 \pm 0.027$
13	470	0.400	$-0.181 \pm 0.022$
14	521	0.434	$-0.227 \pm 0.021$
15	537	0.467	$-0.197 \pm 0.021$
16	493	0.500	$-0.182 \pm 0.023$
17	499	0.534	$-0.067 \pm 0.030$
18	498	0.567	$-0.126 \pm 0.033$
19	453	0.600	$-0.114 \pm 0.029$
20	383	0.634	$0.027 \pm 0.039$
21	368	0.667	$0.086 \pm 0.038$
22	265	0.699	$0.126 \pm 0.042$
23	190	0.733	$0.443 \pm 0.059$
24	106	0.765	$0.366 \pm 0.084$
25	100	0.798	$0.520 \pm 0.093$

**Figure 3.** The black plot shows the average intrinsic magnitude of SDSS quasars as a function of intrinsic wavelength,  $\psi$ . The position of the wavelength for the Lyman $\alpha$  line is shown in blue and that for the hydrogen ionization is shown in red.

407 All quasar data used here is taken from the Sloan Dig-  
 408 ital Sky Survey Quasar Catalog: Sixteenth Data Release  
 409 (DR16Q) Lyke et al. (2020).

410 The majority of these quasars have been discovered  
 411 by a flux density limited survey without knowledge of  
 412 the redshift and it is clear that the observed magnitudes  
 413 have a very limited dependence on their observed red-  
 414 shift. Thus the observation model is that the selection  
 415 of each quasar is determined by the cut-off flux density  
 416 and the overall telescope noise and it is assumed that  
 417 these values are the same for all the quasars.

418 Thus for each quasar discovered its apparent magni-  
 419 tude must lie in the range of magnitudes that are ac-  
 420 cepted by the telescope and it is completely independent  
 421 of the intrinsic magnitude of the quasar. The observed  
 422 flux density depends on the probability of seeing the  
 423 quasar and its distance. Since the observed distance  
 424 is rapidly increasing with redshift, it is proportional to  
 425 the maximum area. For this distance the observed flux  
 426 density is inversely proportional to the same area. Since  
 427 these two areas cancel each other, the expected flux den-  
 428 sity is the cut-off flux density plus, if any, common cos-  
 429 mological flux density.

430 The data for each quasar is its redshift and the ob-  
 431 served magnitudes for the 5 bands,  $UBVRI$ . The in-  
 432 trinsic magnitude for each band is determined by the  
 433 procedure described in section 2.3 for the supernova,  
 434 except there were 1000 boxes.

435 The quasar intrinsic magnitude is shown in Figure 3.  
 436 The rapid decrease in luminosity at short wavelengths

437 is probably due to a local hydrogen cloud. Note that if  
 438 quasars are like black holes then the size of this cloud  
 439 could be very small and it would not easily be detected  
 440 against the luminosity of the accretion disk.

441 If the universe is expanding then this energy loss factor  
 442 is proportional to  $(1+z)^{-1}$ . A simple method to measure  
 443 this average energy loss is to assume that the expected  
 444 magnitude is

$$m = a + b \times 2.5 \log_{10}(1+z) \quad (6)$$

445 Then the expected values are  $a = -1$  and  $b = -1$ .  
 446 The weighted regression equation for 635,218 quasars  
 447 produced the results  $a = -0.9109 \pm 0.001$  and

$$b = -(1.0073 \pm 0.0046). \quad (7)$$

448 The difference of the parameter  $a$  from -1 is unknown  
 449 but fortunately it is not important here. However the  
 450 agreement of parameter  $b$  with -1 is very clear and shows  
 451 very strong support for an energy loss rate of  $1/(1+z)$ .

## 452 2.5. Supernova absolute magnitudes.

453 The absolute magnitude of Type Ia supernova is the  
 454 sum of the apparent magnitude and a distance modulus.

455 Scolnic et al. (2017) suggests several distance moduli  
 456 that have a good fit to the PS1 Medium Deep Survey  
 457 that were analyzed with the SALT2 method. The sim-  
 458 plest is the  $\Lambda$ CDM model. There are two sets of data,  
 459 the 1117 PS1 set and the combined 1652 described above  
 460 that can be used to test the absolute magnitude depen-  
 461 dence on redshift. The PS1 set (JonesJones et al. (2018)  
 462 table (3)) is a list of results from the Pan-STARRS  
 463 supernova survey and their apparent magnitudes have

464 been corrected using Scolnic et al. (2017) Eq.(3) and  
 465 using the oCDM model, the regression of the absolute  
 466 magnitude verse redshift for the 1117 PS1 Type Ia su-  
 467 pernova that used the SALT2 model

$$M(z) = -19.216 \pm 0.009 + (0.052 \pm 0.067)z, \quad (8)$$

468 where the last term is statistically equal to zero. This  
 469 shows that the SALT2 method is consistent with the  
 470 oCDM model.

471 However the regression for the 1652 PS1 Type Ia  
 472 supernova, using the intrinsic analysis and the oCDM  
 473 model, is

$$M(z) = -17.572 \pm 0.009 + (0.669 \pm 0.059)z, \quad (9)$$

474 where the last term is not equal to zero.

### 475 2.6. Discussion of SALT2 supernova magnitudes.

476 The absolute magnitudes of PS1 supernova that are  
 477 analyzed by the SALT2 method and using the oCDM  
 478 model show negligible dependence on redshift. However  
 479 the absolute magnitudes that are obtained from intrinsic  
 480 analysis and using the oCDM model shows a statistically  
 481 valid dependence on redshift,  $\Delta M = (0.833 \pm 0.072)z$   
 482 that is inconsistent with the expected value of zero,

483 could this be due to a fault in the intrinsic analy-  
 484 sis? Because the intrinsic analysis is completely inde-  
 485 pendent of the observed redshift the anomaly must be  
 486 present in the observed data and cannot come from the  
 487 analysis. Although it is not an independent result, sec-  
 488 tion 4.22 shows that there is no Phillip’s relation. The  
 489 conclusion is that it must be in SALT2 and there is a  
 490 corresponding fault in the oCDM procedure that coun-  
 491 terbalances the fault.. As shown in the appendix the  
 492 SALT2 method calibrates a new Type Ia supernova by  
 493 comparing its observations against the results for pre-  
 494 vious supernova measurements, these results only show  
 495 self-consistency and do not provide validation of the flux  
 496 densities. However if there is a systematic error in the  
 497 previous supernova measurements, it will be transmit-  
 498 ted to new observations. Furthermore SALT2 includes  
 499 many ad hoc parameters and it is very complex and in-  
 500 cludes the nuisance parameter  $\alpha$  that is a measure of the  
 501 Phillip’s relation between magnitude and redshift.

502 The major support for the  $\lambda$ CDM model is that it  
 503 describes the general relativity model of an unstable ex-  
 504 panding universe. This is similar to assuming that a  
 505 falling feather should have the same acceleration as a  
 506 falling stone, whereas we know that the difference is due  
 507 to air resistance. Maybe cosmology needs something like  
 508 air resistance such as Curvature-cosmology,

509 Crucially the standard procedure is to use oCDM or  
 510 one of its variants to determine the dimensionless den-

511 sity parameters, which depend on assumptions of infla-  
 512 tion, dark matter and dark energy. Since none of these  
 513 properties are substantiated by other independent ob-  
 514 servations, they do not provide any support for this cos-  
 515 mology. Moreover they are ad hoc models largely deter-  
 516 mined by supernova observations. In other words, there  
 517 are no observations other than those for supernova that  
 518 show strong confirmation of the SALT2 analysis and the  
 519  $\lambda$ CDM model.

## 520 3. PART B: CURVATURE-COSMOLOGY THEORY.

### 521 3.1. Introduction

522 Curvature-cosmology is a static tired-light cosmology  
 523 which is based on the two hypothesizes of Curvature-  
 524 redshift which is based on the propagation of a wave  
 525 in of curved space-time and Curvature-pressure which  
 526 opposes the mutual gravitational attraction of hot gases.

527 It is a static solution to the equation of general relativ-  
 528 ity that is described by the Friedmann equations with an  
 529 additional term that stabilizes the solution. This term  
 530 called Curvature-pressure is a reaction of high-speed  
 531 particles back on the material producing the curved  
 532 space-time. This sense of this reaction is to try and  
 533 reduce the curvature.

534 The basic cosmological model is one in which the cos-  
 535 mic plasma dominates the mass distribution and hence  
 536 the curvature of space-time. In this first-order model,  
 537 the gravitational effects of stars and galaxies are ne-  
 538 glected. The geometry C is that of a three-dimensional  
 539 “surface’ of a four-dimensional hyper-sphere, which is  
 540 common to most cosmologies.

541 For a static universe, there is no ambiguity in the  
 542 definition of distances and times. One can use a uni-  
 543 versal cosmic time and define distances in light travel  
 544 times or any other convenient measure. In a statistical  
 545 sense Curvature-cosmology obeys the perfect cosmolog-  
 546 ical principle of being the same at all places and at all  
 547 times.

548 Curvature-cosmology makes quite specific predictions  
 549 that can be refuted. Thus, any observations that unam-  
 550 biguously show changes in the universe with a redshift  
 551 would invalidate it. In Curvature-cosmology, there is a  
 552 continuous process in which some of the cosmic gas will  
 553 aggregate to form galaxies and then stars. The galaxies  
 554 and stars will evolve and eventually all their material  
 555 will be returned to the cosmic plasma. Thus, a char-  
 556 acteristic of Curvature-cosmology is that although in-  
 557 dividual galaxies will be born, live and die, the overall  
 558 population will be statistically the same for any observ-  
 559 able characteristic.

### 560 3.2. Derivation of Curvature-redshift

561 The derivation of Curvature-redshift is based on the  
 562 fundamental hypothesis of Einstein's general theory of  
 563 relativity that space is curved. As a consequence, the  
 564 trajectories of initially parallel point particles, geodesics,  
 565 will move closer to each other, or further apart as time  
 566 increases. Consequently in space with a positive cur-  
 567 vature, the cross-sectional area of a bundle of geodesics  
 568 will slowly decrease.

569 In applying this idea to photons, we assume that a  
 570 photon is described in quantum mechanics as a local-  
 571 ized wave where the geodesics correspond to the rays of  
 572 the wave. Note that this wave is quite separate from  
 573 an electromagnetic wave that corresponds to the effects  
 574 of many photons. It is fundamental to the hypothesis  
 575 that we can consider the motion in space of individual  
 576 photons.

577 Because the curvature of space causes the focusing of a  
 578 bundle of geodesics, this focusing also applies to a wave.  
 579 As the photon progresses, the cross-sectional area of the  
 580 wave associated with it will decrease. However, in quan-  
 581 tum mechanics properties such as angular momentum  
 582 are computed by an integration of a radial coordinate  
 583 over the volume of the wave and will be affected by the  
 584 focusing.

585 If the cross-sectional area of the wave decreases, then  
 586 the angular momentum will also decrease. However, angu-  
 587 lar momentum is a quantized parameter that for pho-  
 588 tons has a fixed value. The solution to this dilemma  
 589 is that, from symmetry, the photon splits into two very  
 590 low-energy photons and a third that has the same direc-  
 591 tion as the original photon and nearly all the energy.

592 Since in quantum mechanics protons and other parti-  
 593 cles are considered as waves, a similar process will also  
 594 apply. It is argued that protons and other particles will  
 595 interact with curved space to lose energy by the emission  
 596 of very low-energy photons.

597 Einstein's general theory of relativity requires that the  
 598 metric of space-time be determined by the distribution  
 599 of mass (and energy). In general this space-time will be  
 600 curved such that in a space of positive curvature, nearby  
 601 geodesics that are initially parallel will come closer to-  
 602 gether as the reference position moves along them. This  
 603 is directly analogous to the fact that on the earth lines  
 604 of longitude come closer together as they go from the  
 605 equator to either pole. In flat space-time, the separa-  
 606 tion remains constant.

607 The *equation for geodesic deviation* can be written  
 608 Misner, Thorne, & Wheeler (1973) as

$$\frac{d^2\xi}{dr^2} = -\frac{\xi}{R^2},$$

609 where  $\xi$  is a distance normal to the trajectory and  $r$  is  
 610 measured along the trajectory. The quantity  $1/R^2$  is the  
 611 Gaussian curvature at the point of consideration.

612 The experiment of using single photons in a two-slit  
 613 interferometer shows that individual photons must have  
 614 a finite size. Quantum mechanics requires that all par-  
 615 ticles are described by wave functions and therefore we  
 616 must consider the propagation of a wave in space-time.  
 617 Because photons are bosons, the usual quantum me-  
 618 chanical approach is to describe the properties of pho-  
 619 tons by creation and destruction operators.

620 However, in any other reference frames they behave  
 621 like normal particles with definite trajectories and life-  
 622 times. Although Havas (1966) has pointed out that the  
 623 concept of a single photon is rather tenuous. There is no  
 624 way we can tell the difference between a single photon  
 625 and a bundle of photons with the same energy, momen-  
 626 tum, and spin. Nevertheless, it is an essential part of  
 627 this derivation that a single photon has an actual exist-  
 628 ence.

629 Assume that a photon can be described by a local-  
 630 ized wave packet that has finite extent both along and  
 631 normal to its trajectory. This economic description is  
 632 sufficient for the following derivation. From de Broglie's  
 633 equation the frequency of a photon with energy  $E$  is  
 634  $\nu = E/h$  and its wavelength as  $\lambda = hc/E$  where  $E$  is its  
 635 energy. These definitions are for convenience and do not  
 636 imply that we can ascribe a frequency or a wavelength  
 637 to an individual photon; they are properties of groups of  
 638 photons. The derivation requires that the wavelength is  
 639 short compared to the size of the wave packet and that  
 640 this is short compared to variations in the curvature of  
 641 space-time.

642 Furthermore, we assume that the rays follow null  
 643 geodesics and therefore any deviations from flat space-  
 644 time produce change in shape of the wave packet. In  
 645 other words, since the scale length of deviations from flat  
 646 space are large compared to the size of the wave packet  
 647 they act as a very small perturbation to the propagation  
 648 of the wave packet.

649 Consider a wave packet moving through a space-time  
 650 of constant positive curvature. Because of geodesic de-  
 651 viation, the rays come closer together as the wave packet  
 652 moves forward. They are focused. In particular the di-  
 653 rection  $\theta$ , of a ray (geodesic) with initial separation  $\xi$   
 654 after a distance  $r$  is (assuming small angles)

$$\theta = -\frac{r\xi}{R^2},$$

655 where  $R$  is the radius of curvature.

656 Since the central geodesic is the direction of energy  
 657 flow, we can integrate the wave-energy-function times  
 658 the component of  $\theta$  normal to the trajectory, over the



659 dimensions of the wave packet in order to calculate the  
 660 amount of energy that is now traveling normal to the  
 661 trajectory. The result is a finite energy that depends  
 662 on the average lateral extension of the wave packet, the  
 663 local radius of curvature, and the original photon energy.

664 The actual value is not important but rather the fact  
 665 that there is a finite fraction of the energy that is mov-  
 666 ing away from the trajectory of the original wave packet.  
 667 This suggests a photon interaction in which the pho-  
 668 ton interacts with curved space-time with the hypoth-  
 669 esis that the energy flow normal to the trajectory goes  
 670 into the emission of secondary photons normal to its  
 671 trajectory.

672 From a quantum-mechanical point of view, there is a  
 673 strong argument that some interaction must take place.  
 674 If the spin of the photon is directly related to the angular  
 675 momentum of the wave packet about its trajectory then  
 676 the computation of the angular momentum is a similar  
 677 integral.

678 Then because of *focussing* the angular momentum  
 679 clearly changes along the trajectory, which disagrees  
 680 with the quantum requirement that the angular momen-  
 681 tum, that is the spin, of the photon is constant. The  
 682 Heisenberg uncertainty principle requires that an incor-  
 683 rect value of spin can only be tolerated for a small time  
 684 before something happens to restore the correct value.  
 685 We now consider the consequences.

686 Consider motion on the surface of a three-dimensional  
 687 sphere with radius  $r$ . As described above, two adjacent  
 688 geodesics will move closer together due to focusing. Sim-  
 689 ple kinematics tells us that a body with velocity  $v$  asso-  
 690 ciated with these geodesics has acceleration  $v^2/r$ , where  
 691  $r$  is the radius of curvature. This acceleration is directly  
 692 experienced by the body.

693 The geometry of a three-dimensional ‘surface’ with  
 694 curvature in the fourth dimension is essentially the same  
 695 as motion in three dimensions except that the focusing  
 696 now applies to the cross-sectional area and not to the  
 697 separation.

698 Since wave packet that is subject to focusing has ac-  
 699 celeration in an orthogonal dimension will also experi-  
 700 ence an acceleration of  $c^2/r$  normal to the surface of the  
 701 sphere. Then a wave packet (and hence a photon) that  
 702 has its cross-sectional area focused by curvature in the  
 703 fourth dimension with radius  $r$  would have an energy  
 704 loss rate proportional to this acceleration. The essence  
 705 of the Curvature-redshift hypothesis is that the focus-  
 706 ing causes the photon to interact and that the energy  
 707 loss rate is proportional to  $c^2/R$ . For a photon with en-  
 708 ergy  $E$  the loss rate per unit time is  $cE/R$ , and per unit  
 709 distance it is  $E/R$ .

710 In general relativity the crucial equation for the focus-  
 711 ing of a bundle of geodesics was derived by Raychaud-  
 712 huri (1955), also see Misner et al. (1973) and Ellis (1984)  
 713 and for the current context we can assume that the bun-  
 714 dle has zero shear and zero vorticity. Since any change  
 715 in geodesic deviation along the trajectory will not alter  
 716 the direction of the geodesics, we need consider only the  
 717 cross-sectional area  $A$  of the geodesic bundle to get the  
 718 equation

$$\frac{1}{A} \frac{d^2 A}{dr^2} = -\mathbf{R}_{\alpha\beta} \mathbf{U}^\alpha \mathbf{U}^\beta = -\frac{1}{R^2}, \quad (10)$$

719 where  $\mathbf{R}$  is the Ricci tensor (it is the contraction of the  
 720 Riemann-Christoffel tensor),  $\mathbf{U}$  is the 4-velocity of the  
 721 reference geodesic and  $R$  is the local radius of curva-  
 722 ture. This focusing can be interpreted as the second  
 723 order rate of change of cross-sectional area of a geodesic  
 724 bundle that is on the three-dimensional surface in four-  
 725 dimensional space. Then if we consider that a photon is  
 726 a wave packet we find that the rate at which the photon  
 727 loses energy per unit distance is  $E/R$  or more explicitly.

$$\frac{1}{E} \frac{dE}{dr} = -\frac{1}{R} = -(\mathbf{R}_{\alpha\beta} \mathbf{U}^\alpha \mathbf{U}^\beta)^{1/2}, \quad (11)$$

728 What is interesting about this equation is that, for the  
 729 Schwarzschild (and Kerr) solutions for the external field  
 730 for a mass, the Ricci tensor is zero; hence, there is no  
 731 focusing and no energy loss. A geodesic bundle passing  
 732 a mass such as the sun experiences a distortion but the  
 733 wave packet has not changed in area. Hence, this model  
 734 predicts that photons passing near the limb of the sun  
 735 will not suffer any energy loss due to curvature-redshift.

### 3.3. Gravitation is not a force

736  
 737 The phrase *gravitational force* is not only a popular  
 738 expression but is endemic throughout physics. In par-  
 739 ticular, gravitation is classified as one of the four funda-  
 740 mental forces with its heritage going back to Newton’s  
 741 law of gravitation. I argue that the formulation of grav-  
 742 itation as a force is a misconception. In both Newtonian  
 743 theory and general relativity, gravitation is acceleration.  
 744 To begin let us examine the original Newtonian gravita-  
 745 tion equation.

$$m_I \mathbf{a} = \mathbf{F} = -\frac{GMm_G}{r^3} \mathbf{r}, \quad (12)$$

746 where (following Longair (1991)) we identify  $m_I$  as the  
 747 inertial mass of the test object,  $M$  as the active gravita-  
 748 tional mass of the second object and  $m_G$  as the passive  
 749 gravitational mass of the test object. The vector  $\mathbf{a}$  is its  
 750 acceleration and  $\mathbf{r}$  is its displacement from the second  
 751 object. This equation is usually derived in two steps:

752 first, the derivation of a gravitational field and second, 801  
 753 the force produced by that field on the test mass. By 802  
 754 analogy with Coulomb’s law, the passive gravitational 803  
 755 mass has a similar role to the electric charge. 804

756 However many experiments by Eötvös, Pekár, & 805  
 757 Fekete (1922), Dicke (1964), and Braginskij & Panov 806  
 758 (1971) have shown that the passive gravitational mass 807  
 759 is equal to the inertial mass to about one part in  $10^{12}$ . 808  
 760 The usual interpretation of the agreement is that they 809  
 761 are fundamentally the same thing. However, an alterna- 810  
 762 tive viewpoint is that the basic equation is wrong and 811  
 763 that the passive gravitational mass and the inertial mass 812  
 764 should not appear in the equation. In this case the cor-  
 765 rect equation is

$$\mathbf{a} = -\frac{GM}{r^3}\mathbf{r}. \quad (13)$$

766 Thus, the effect of gravitation is to produce accelera-  
 767 tions directly; there is no force involved. Some might  
 768 argue that since the two masses cancel the distinction is  
 769 unimportant. On the other hand, I would argue that the  
 770 application of Ockham’s razor dictates the use of Eq. 13  
 771 instead of Eq. 12.

772 The agreement of the inertial mass with the passive  
 773 gravitational mass is the basis of the weak equivalence  
 774 principle in that it applies regardless of the composition  
 775 of the matter used. Carlip (1998) Shows that it applies  
 776 to both the potential and the kinetic energy in the body.  
 777 The theory of general relativity is based on the principle  
 778 of equivalence as stated by Einstein: *All local, freely*  
 779 *falling, non-rotating laboratories are fully equivalent for*  
 780 *the performance of physical experiments.*

781 The relevance here is that it is impossible to distin-  
 782 guish between acceleration and a uniform gravitational  
 783 field. Thus when gravitation is considered as accelera-  
 784 tion and not a force the passive gravitational mass is a  
 785 spurious quantity that is not required by either theory.

### 786 3.4. Derivation of Curvature-pressure.

787 The hypothesis of Curvature-pressure is that for mov-  
 788 ing particles there is a pressure generated that acts back  
 789 on the matter that causes the curved space-time. In this  
 790 case, Curvature-pressure acts on the matter (plasma)  
 791 that is producing curved space-time in such a way as  
 792 to try to decrease the curvature. In other words, the  
 793 plasma produces curved space-time through its den-  
 794 sity entering the stress-energy tensor in Einstein’s field  
 795 equations and the constraint of the plasma to a three-  
 796 dimensional hyper-“surface”.

797 A simple cosmological model using Newtonian physics  
 798 in four-dimensional space illustrates some of the ba-  
 799 sic physics subsequently used to derive the features  
 800 of Curvature-pressure. The model assumes that the

801 universe is composed of plasma confined to the three-  
 802 dimensional “surface” of a four-dimensional hypersphere.

803 Since the visualization of four dimensions is difficult  
 804 let us suppress one of the normal dimensions and con-  
 805 sider the gas to occupy the two-dimensional surface of a  
 806 normal sphere. From Gauss’s law (i.e. the gravitational  
 807 effect of a spherical distribution of particles with radial  
 808 symmetry is identical to that of a point mass equal in  
 809 value to the total mass situated at the center of symme-  
 810 try) the gravitational acceleration at the radius  $r$  of the  
 811 surface is normal to the surface, directed inward and it  
 812 has the magnitude

$$\ddot{r} = -\frac{GM}{r^2}, \quad (14)$$

813 where  $M$  is the total mass of the particles and the dots  
 814 denote a time derivative. For equilibrium, and assuming  
 815 all the particles have the same mass and velocity we  
 816 can equate the radial acceleration to the gravitational  
 817 acceleration and get the simple equation from celestial  
 818 mechanics of

$$\frac{v^2}{r} = \frac{GM}{r^2}.$$

819 If there is conservation of energy, this stable situation is  
 820 directly analogous to the motion of a planet about the  
 821 sun.

822 When there is a mixture of particles with different  
 823 masses, there is an apparent problem. In general, parti-  
 824 cles will have a distribution of velocities and the heavier  
 825 ones can be expected to have, on average, lower veloci-  
 826 ties. Thus, equilibrium radii will vary with the velocity  
 827 of the particles.

828 However, the basis of this model is that all particles  
 829 are constrained to have the same radius regardless of  
 830 their mass or velocity with the value of the radius set  
 831 by the average radial acceleration. Thus for identical  
 832 particles with a distribution of velocities we average over  
 833 the squared velocities to get

$$\langle v^2 \rangle = \frac{GM}{r}. \quad (15)$$

834 If there is more than one type of particle with different  
 835 masses then we invoke the precepts of Section 3.3 and  
 836 average over the accelerations to get the same result.  
 837 The effect of this balancing of the accelerations against  
 838 the gravitational potential is seen within the shell as a  
 839 Curvature-pressure that is a direct consequence of the  
 840 geometric constraint of confining the particles to a shell.

841 If the radius  $r$  decreases then there is an increase in  
 842 this Curvature-pressure that attempts to increase the  
 843 surface area by increasing the radius. For a small change  
 844 in radius in a quasi-equilibrium process where the par-  
 845 ticle velocities do not change the work done by this

846 Curvature-pressure (two dimensions) with an incremen-  
 847 tal increase of area  $dA$  is  $p_c dA$  and this must equal the  
 848 gravitational force times the change in distance to give

$$p_c dA = \frac{GM^2}{r^2} dr,$$

849 where  $M = \sum m_i$  with the sum going over all the par-  
 850 ticles and the negative sign shows that it is opposite  
 851 in effect to thermodynamic pressure. Therefore, using  
 852 Eq. 15 we can rewrite the previous equation in terms of  
 853 the velocities as

$$p_c dA = \frac{M \langle v^2 \rangle}{r} dr.$$

854 Now  $dA/dr = 2A/r$ , hence the two-dimensional  
 855 Curvature-pressure is

$$p_c = \frac{M \langle v^2 \rangle}{2A}.$$

856 This simple Newtonian model provides a guide as to  
 857 what the Curvature-pressure would be in the full general  
 858 relativistic model.

859 In deriving a more general model in analogy to the  
 860 Newtonian one, we first change  $dA/dr = 2A/r$  to  
 861  $dV/dr = 3V/r$  (where  $V$  is the volume) and secondly  
 862 we include the correction  $\gamma^2$  needed for relativistic ve-  
 863 locities which refers to the dominant massive particles.  
 864 The result is

$$p_c = \frac{\langle \beta^2 \rangle Mc^2}{3V} = \frac{\langle \gamma^2 - 1 \rangle Mc^2}{3V}. \quad (16)$$

865 Note that the 3 is the number of degrees of freedom.  
 866 In this case the constraint arises from the confinement  
 867 of all the particles within a three-dimensional hyper-  
 868 ‘surface’. Now we expect to be dealing with fully ionized  
 869 high temperature plasma with a mixture of electrons,  
 870 protons, and heavier ions where the averaging is done  
 871 over the accelerations. Define the average density by  
 872  $\rho = M/V$  then the cosmological Curvature-pressure is

$$p_c = \frac{1}{3} \langle 1 - \gamma^2 \rangle \rho c^2. \quad (17)$$

873 In effect, my hypothesis is that the cosmological model  
 874 must include this Curvature-pressure as well as ther-  
 875 modynamic pressure. Note that although this has a  
 876 similar form to thermodynamic pressure it is quite dif-  
 877 ferent. In particular, it is proportional to an average  
 878 over the squared velocities and the thermodynamic pres-  
 879 sure is proportional to an average over the kinetic en-  
 880 ergies. This means that, for plasma with free electrons  
 881 and approximate thermodynamic equilibrium, the elec-  
 882 trons will dominate the average due to their much larger

883 velocities. From a Newtonian point of view, Curvature-  
 884 pressure is opposed to gravitational mutual acceleration.

885 In general relativity, the plasma produces curved  
 886 space-time through its density entering the stress-energy  
 887 tensor in Einstein’s field equations. Then the constraint  
 888 of confining the particles to a three-dimensional shell  
 889 produces a pressure whose reaction is the Curvature-  
 890 pressure acting to decrease the magnitude of the curva-  
 891 ture and hence decrease the density of the plasma.

### 892 3.5. The Curvature-cosmological model

893 Curvature-cosmology can now be derived by includ-  
 894 ing Curvature-redshift and Curvature-pressure into the  
 895 equations of general relativity. This is done by using ho-  
 896 mogeneous isotropic plasma as a model for the real uni-  
 897 verse. The general theory of relativity enters through  
 898 the Friedmann equations for a homogeneous isotropic  
 899 gas.

900 Although such a model is simple compared to the real  
 901 universe, the important characteristics of Curvature-  
 902 cosmology can be derived by using this model. The  
 903 first step is to obtain the basic relationship between the  
 904 density of the gas and the radius of the universe. The  
 905 inclusion of Curvature-pressure is not only important  
 906 in determining the basic equations but it also provides  
 907 the necessary means of making the solution static and  
 908 stable.

909 Then it is shown that the effect of Curvature-redshift  
 910 is to produce a redshift that is a function of distance,  
 911 and the slope of this relationship is (in the limit of small  
 912 distances) the Hubble constant.

913 The first-order model considers the universe to be a  
 914 gas with uniform density and complications such as den-  
 915 sity fluctuations, galaxies, and stars are ignored. In ad-  
 916 dition, we assume (to be verified later) that the gas is  
 917 at high temperature and is fully ionized plasma. Be-  
 918 cause of the high symmetry, the appropriate metric is  
 919 the one that satisfies the equations of general relativity  
 920 for a homogeneous, isotropic gas.

921 Based on the Robertson-Walker metric, the Fried-  
 922 mann equations for the homogeneous isotropic model  
 923 with constant density and pressure without the cosmo-  
 924 logical constant and with  $k = 1$  are (Longair 1991)

$$\begin{aligned} \dot{R}^2 &= \frac{8\pi G\rho}{3} R^2 - c^2 & (18) \\ \ddot{R} &= -\frac{4\pi G}{3} \left( \rho + \frac{3p}{c^2} \right) R, \end{aligned}$$

925 where  $R$  is the radius,  $\rho$  is the density,  $p$  is the ther-  
 926 modynamic pressure,  $G$  is the Newtonian gravitational  
 927 constant and the superscript dots denote time deriva-  
 928 tives.

Assuming that the thermodynamic pressure is negligible and including the Curvature-pressure, Eq. 17, the second modified Friedmann equation is

$$\ddot{R} = -\frac{4\pi G\rho}{3} [1 + \langle 1 - \gamma^2 \rangle] R, \quad (19)$$

Clearly, there is a static solution with  $\ddot{R} = 0$  which means that  $\gamma^2 = 2$ .

The first Friedmann equation provides the radius of the universe which is

$$\begin{aligned} R &= \sqrt{\frac{3c^2}{8\pi G\rho}} \text{ m} \\ &= 1.268 \times 10^{13} / \sqrt{\rho} \text{ m} \\ &= 3.112 \times 10^{26} / \sqrt{N_e} \text{ m} \\ &= 1.008 \times 10^4 / \sqrt{N_e} \text{ Mpc} \end{aligned} \quad (20)$$

where  $N_e$  is the number density measured in number of hydrogen atoms per  $\text{m}^3$ .

The basic instability of the static Einstein model is well known (Tolman 1934; Ellis 1984). On the other hand, the effect of Curvature-pressure is opposite in effect to the normal pressure thus Curvature-cosmology is intrinsically stable.

Now the apparent ‘velocity’,  $v(z)$  is the rate of change of  $z$  and by definition  $dr/dt = c$ , thus

$$v(z) = \frac{dz}{dt} = c \frac{dz}{dr} = \frac{c(1+z)}{R}. \quad (21)$$

Since Hubble’s equation is equal to this velocity it is

$$H(z) = \frac{c(1+z)}{R}, \quad (22)$$

and Hubble’s constant is  $H_0 = c/r$  and has the value

$$H_0 = c/R \text{ s}^{-1} \quad (23)$$

$$\begin{aligned} &= 2.364 \times 10^{-5} \sqrt{\rho} \text{ s}^{-1} \\ &= 9.6352 \times 10^{-19} \sqrt{N_e} \text{ s}^{-1} \\ &= 29.73 \sqrt{N_e} \text{ kms}^{-1} \text{ Mpc}^{-1} \\ &= 41.30 \text{ kms}^{-1} \text{ Mpc}^{-1}, \end{aligned} \quad (24)$$

where the last line has used  $N_e = 1.93$  from section 4.2.

Since  $E = ch/\lambda$  and with the redshift and using Eq. 11 provides an important equation which shows the relationship between the cosmic distance and redshift and is

$$\log(E(r)/E_0) = -r/R. \quad (25)$$

Since  $z = (\lambda/\lambda_0 - 1)$  then

$$r = R \log(1+z). \quad (26)$$

Integration provides an alternative form for the energy loss which is

$$z = \exp(-r/R) - 1. \quad (27)$$

Of interest is that the distance to the furthest point is  $r/R = \pi$  which has a redshift of  $z = 22.141$ . The light travel time to that point is  $\pi R/c = 7.439 \times 10^{10}$  years.

### 3.6. Distance modulus.

The geometry of Curvature-cosmology is that of a three-dimensional ‘surface’ of a four-dimensional hypersphere with radius  $R$ . For this geometry the area is

$$A(r) = 4\pi[R \sin(r/R)]^2.$$

Let a source have a luminosity  $L(\nu)$  ( $\text{W Hz}^{-1}$ ) at the emission frequency  $\nu$ . Then if energy is conserved, the observed flux density,  $F(\nu)$  ( $\text{W m}^{-2} \text{ Hz}^{-1}$ ) at a distance parameter  $z$  is the luminosity divided by the area, which is

$$F(\nu)d\nu = \frac{L(\nu) d\nu}{4\pi[R \sin(r/R)]^2}.$$

However, because of Curvature-redshift there is an energy loss such that the received frequency  $\nu_0$  is related to the emitted frequency  $\nu_e$  by  $(\nu_0 = (1+z)\nu_e)$ . Including this the result and Eq. 25 it is

$$F(\nu_0)d\nu_0 = \frac{L(\nu_0) d\nu_0}{4\pi[R \sin(\log(1+z))]^2(1+z)}.$$

since the absolute magnitude is the apparent magnitude when the object is at a distance of 10 pc then

$$F_{10}(\nu_0) d\nu_0 = \frac{1}{10\text{pc}/R},$$

where because 10 pc is negligible compared to  $R$ , approximations have been made. The flux density ratio is

$$F(\nu_0) = \left[ \frac{10\text{pc}/R}{\sin(\log(1+z))} \right]^2 \left\{ \frac{1}{1+z} \right\}.$$

The apparent magnitude is defined as  $m = -2.5 \log(S)$  where the base of the logarithm is 10 and the constant 2.5 is exact and  $M$  as the absolute magnitude we get the distance modulus,  $\mu = m - M$  to be

$$\mu = 5 \log_{10}[R \sin(\log(1+z))] + 2.5 \log_{10}(1+z) + 44.304. \quad (28)$$

### 3.7. Temperature of the cosmic plasma

One of the most remarkable results of Curvature cosmology is that it predicts the temperature of the cosmic plasma from fundamental constants. That is the predicted temperature is only dependent on the electron density of the intra-galactic medium.

For a stable solution to Eq. 19 we need that  $\langle \gamma^2 \rangle = 2$ , where the average (denoted by  $\langle \rangle$ ) is taken over the proton number densities. Since the total energy for a particle is  $\gamma mc^2$  the kinetic energy is  $E(\gamma - 1)mc^2$ . In this case for protons  $E = 3.391E^{-14}$  J and from  $E = kT$  the plasma temperature is

$$T = 2.456E9. \quad (29)$$

Since electrons and nucleons have wave properties there are subject to Curvature-redshift where the basic energy loss is  $\Delta E = E_0 r/R$ , where  $E_0$  is the particle energy and  $r$  is the distance traveled. With a velocity of  $\beta c$  the distance traveled is  $r = \beta ct$  and the rate of energy loss is

$$\frac{\Delta E}{dt} = \frac{E_0 \beta c}{R} \quad (30)$$

The distribution of relativistic particles in equilibrium is the Maxwell-Jöoner distribution. With  $\gamma = 1/\sqrt{1 - v^2/c^2}$  it is

$$f(\gamma) = \frac{\gamma^2 \beta}{\theta K_2(1/\theta)} \exp(-\gamma/\theta), \quad (31)$$

where  $\theta = kT/mc^2$  and  $K_2$  is the modified Bessel function of the second kind.

Here its application requires that  $\theta$  is a constant value then the integral over the range of  $\gamma$  is

$$\frac{\Delta E}{dt} = \frac{\gamma^2 \beta^2 c(\gamma - 1)m_p c^2}{R} \exp(-\gamma/\gamma_0)/A, \quad (32)$$

where  $A$  is the normalization constant and is

$$A = \int_1^\infty \gamma^2 \beta(\exp(-\gamma/\gamma_0)) d\gamma, \quad (33)$$

and where  $\gamma_0 = \sqrt{2}$ .

As explained earlier this lost energy consists of a pair of identical photons whose usual interaction with the electrons and photons bring them into thermal equilibrium. Since the total energy must be conserved, the energy lost by Curvature-redshift must be radiated by the emittance of these photons. Then allowing for the nucleon number density  $N_\epsilon = 1.93$ , section 4.2, their equilibrium temperature is 2.736K. It will be argued in section 4.3 that this radiation is the cosmic microwave background radiation.

Clearly, the same analysis can be applied to the free electrons. In this case the radiation has a temperature of 0.419K with a wavelength of 34.4mm.

### 3.8. Black holes and Jets

Consider a very small homogeneous mass with a radius  $R$ . Its dynamics are described by the Friedmann

equations, Eq. 18, and if the acceleration is zero then  $\dot{R} = 0$  and

$$\frac{8\pi G \rho_0 R_0^2}{3} = c^2,$$

where  $\rho_0 = 3m/(4\pi R_0^3)$  is the density. Then the minimum radius is

$$R_0 = \frac{2Gm}{c^2}. \quad (34)$$

For a simple theoretical black hole, this is the Schwarzschild radius.

Since the acceleration is zero, there is an absolute minimum radius and smaller radii are inaccessible. This object has all the external properties of a black hole, such as accretion disks. Thus it looks like the theoretical black hole but is not a black hole.

If the compact object is rotating there is the tantalizing idea that Curvature-pressure may produce the emission of material in two jets along the spin axis. Since the object will be radiating energy all the time, after climbing out of the gravitational pit it will have a similar temperature to the object before it started to collapse. The limiting distance will be determined by the polar radius. Thus radii greater than this, such as the equatorial radii will still be able to emit energy that can be seen. Thus the object will appear like a doughnut with zero radiation at the center and with a very broad jet parallel to the spin axis.

This could be the 'jet engine' that produces the astrophysical jets seen in stellar-like objects and in many huge radio sources. Currently there are no accepted models for the origin of these jets.

### 3.9. Inhibition of Curvature-redshift

from the discussion above it is clear that the process of Curvature-redshift requires a gradual focusing to a critical limit, followed by the emission of secondary photons. It is as if the photon gets slowly excited by the focusing until the probability of secondary emission becomes large enough for it to occur.

If there is any other interaction the excitation due to focusing will be nullified. That is, roughly speaking, Curvature-redshift interaction requires an undisturbed path length of at least  $\lambda_{secondary}$  for the interaction to occur. Thus suitable criterion for inhibition to occur is that the competing interaction has an interaction length less than  $\lambda_{secondary}$ .

Although Compton or Thompson scattering are possible inhibitors, there is another interaction that has a much larger cross-section. This is the coherent multiple scattering that produces refractive index.

In classical electromagnetic theory, the refractive index of a medium is the ratio of the velocity of light



in vacuum to the group velocity in the medium. However, in quantum mechanics photons always travel at the velocity of light in vacuum. In a medium, a group of photons appears to have a slower velocity because the individual photons interact with the electrons in the medium and each interaction produces a time delay.

Because the interaction of a photon is with many electrons spread over a finite volume, the only possible result of each interaction is the emission of another photon with the same energy and momentum. Now consider the absorption of a wave. In order to cancel the incoming wave a new wave with the same frequency and amplitude but with opposite phase must be produced. Thus, the outgoing wave will be delayed by half a period with respect to the incoming wave. If the phase difference was not exactly half a period for an electromagnetic wave incident on many electrons, the principle of conservation of energy would be violated.

This simple observation enables us to compute the interaction length for refractive index  $n$ . If  $L$  is this interaction length then it is

$$L = \frac{\lambda_0}{2|n - 1|},$$

where  $n$  is the refractive index and the modulus allows for plasma and other materials where the refractive index is less than zero.

Note that  $L$  is closely related to the extinction length derived by Ewald and Oseen (see (Jackson 1975) or Born & Wolf (1999)) which is a measure of the distance needed for an incident electromagnetic wave with velocity  $c$  to be replaced by a new wave.

For plasmas the refractive index is

$$n \cong 1 - \frac{N_e \lambda_0^2}{2\pi r_0},$$

where  $N_e$  is the electron density and  $r_0$  is the classical electron radius. We can combine these two equations to get (for a plasma)

$$L = (N_e r_0 \lambda_0)^{-1}. \quad (35)$$

Thus, we would expect the energy loss to be inhibited if the average Curvature-redshift interaction distance is greater than that for refractive-index interactions. Therefore, we can compute the ratio (assuming a plasma with  $N \cong N_e$ ) to get

$$\lambda_{secondary}/L = 0.0106 N_e^{3/4} \lambda_0^{3/2} \quad (36)$$

This result shows that Curvature-redshift will be inhibited if this ratio is greater than one, which is equivalent to  $\lambda_0 \geq 20.7 N_e^{-1/2}$  m. For example, Curvature-redshift for the 21 cm hydrogen line will be inhibited if the electron density is greater than about  $10^4 \text{ m}^{-3}$ .

### 3.10. Possible laboratory tests.

It is apparent from the above analysis that to observe the redshift in the laboratory we need to have sufficient density of gas (or plasma) to achieve a measurable effect but not enough for there to be inhibition by the refractive index.

The obvious experiment is to use the Mössbauer effect for  $\gamma$ -rays that enable very precise measurement of their frequency. Simply put, the rays are emitted by nuclei in solids where there is minimal recoil or thermal broadening of the emitted ray.

Since the recoil momentum of the nucleus is large compared to the atomic thermal energies and since the nucleus is locked into the solid so that the recoil momentum is precisely defined, then the  $\gamma$ -ray energy is also precisely defined. The absorption process is similar and has a very narrow line width.

Such an experiment has already been done by Pound & Snider (1965). They measured gravitational effects on 14.4 keV  $\gamma$ -rays from  $^{57}\text{Fe}$  being sent up and down a vertical path of 22.5m in helium near room pressure. They found agreement to about 1% with the predicted fractional redshift of  $1.5 \times 10^{-15}$ , whereas fractional Curvature-redshift predicted by Eq. 11 for this density is  $1.25 \times 10^{-12}$ . Clearly, this is much larger.

At  $\gamma$ -ray frequencies, the electrons in the helium gas are effectively free and we can use Eq. 35 to compute the refractive index interaction length. For helium at STP, it is  $L = 0.077$  m, which is much less than Curvature-redshift interaction length which for these conditions is  $X=11$  m. Hence, we do not expect to see any significant Curvature-redshift in their results.

Pound and Snyder did observe one-way frequency shifts but they were much smaller than Curvature-redshift and could be explained by other aspects of the experiment. However, the Pound and Snyder experiment provide a guide to a possible test for the existence of Curvature-redshift. Because Curvature-redshift has a different density variation to that for the inhibiting refractive index it is possible to find a density for which Curvature-redshift is not inhibited.

Although there is a slight advantage in using heavier gases than helium due to their higher atomic number to atomic weight ratio, their increased absorption to  $\gamma$ -rays rules them out. Hence, we stay with helium and from Eq. 35 we can compute Curvature-redshift interaction length to be

$$X = 10.8 \left( \frac{p_0}{p} \right)^{1/4} \text{ m},$$

where  $p$  is the pressure and  $p_0$  is the pressure at STP. For the same gas the refractive-index interaction length

1163 is

$$L = 0.077 \left( \frac{p_0}{p} \right) \text{ m.}$$

1164 It follows that the Curvature-redshift will not be in-  
 1165 hibited if  $X < L$  or in this case, the pressure is less than  
 1166  $0.0014p_0$  which is about 1 mm of Hg. For this pressure,  
 1167 we find that  $X = 57$  m which requires that the appa-  
 1168 ratus must be much longer than 57 m. For argument  
 1169 let us take the length to be 100 m then the fractional  
 1170 redshift expected is  $2.1 \times 10^{-13}$  which is detectable.

1171 The experimental method would use a horizontal (to  
 1172 eliminate gravitational redshifts) tube filled with helium  
 1173 and with accurately controlled temperature. Then we  
 1174 would measure the redshift as a function of pressure.  
 1175 The above theory predicts that if it is free of inhibition  
 1176 then the redshift should be proportional to the square  
 1177 root of the pressure.

1178 Alternatively, it may be possible to detect the sec-  
 1179 ondary photons. For helium with a pressure of 1 mm  
 1180 Hg the expected frequency of the secondary radiation  
 1181 from  $^{57}\text{Fe}$  is about 100 kHz. The expected power from  
 1182 a 1 Cu source is about  $5 \times 10^{-22}$  W. Unfortunately, the  
 1183 secondary radiation could be spread over a fairly wide  
 1184 frequency band which makes its detection somewhat dif-  
 1185 ficult but it may be possible to detect the radiation with  
 1186 modulation techniques.

## 1187 4. PART C: OBSERVATIONS

### 1188 4.1. Type Ia supernova

1189 For the 1,652 Type Ia supernova analyzed in Part A  
 1190 the light curve width is

$$w_{obs}(z) = 1.060 \pm 0.009 + (1.080 \pm 0.042) z, \quad (37)$$

1191 which shows an excellent agreement with the expected  
 1192  $(1+z)$  width dependence.

1193 The distribution of the apparent magnitudes is shown  
 1194 in Figure 4. and the regression of the absolute magni-  
 1195 tude as a function of redshift for Curvature-cosmology  
 1196 is  
 1197

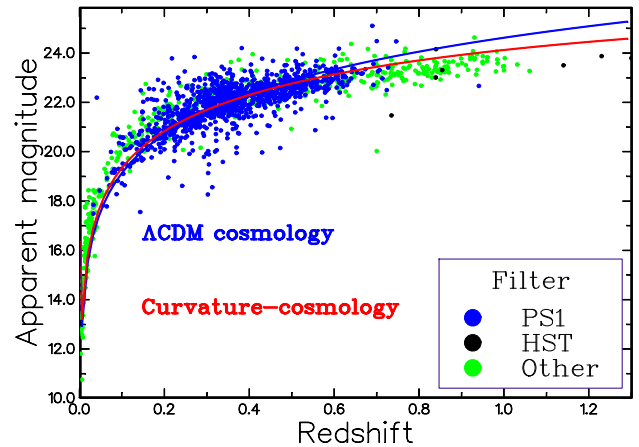
$$M(z) = -17.597 \pm 0.012 + (0.143 \pm 0.057) z,$$

1198 which also shows excellent agreement with a constant  
 1199 value.

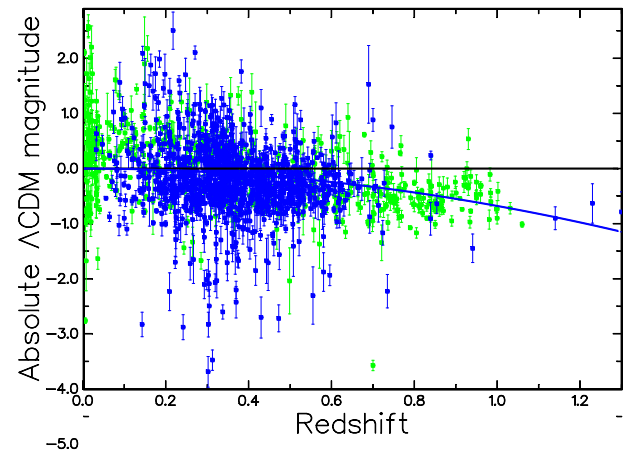
1200 However as shown in section 2.5 the regression for the  
 1201 1652 Type Ia supernova, using the intrinsic analysis and  
 1202 the  $\Lambda$ CDM model, is

$$M(z) = -17.572 \pm 0.009 + (0.669 \pm 0.059) z. \quad (38)$$

1203 It was argued there that this is because of a fault in the  
 1204 SALT2 analysis.



1205 **Figure 4.** The cosmological apparent magnitude of the  
 1206 current Type Ia supernova as a function of redshift. The blue  
 1207 curve is the distance modulus for the  $\Lambda$ CDM model. The red  
 1208 curve is the distance modulus for Curvature-cosmology.



1209 **Figure 5.** The absolute magnitude of the current Type Ia  
 1210 supernova as a function of redshift for the  $\Lambda$ CDM model.  
 1211 The blue curve shows the dark energy magnitude change of  
 1212  $(0.697 \pm 0.064)z^2$ . The legend is the same as for Figure 4

1206 In the standard model, this result is said to be the  
 1207 consequence of dark energy that increases the apparent  
 1208 velocity at large redshifts. For this set of Type Ia super-  
 1209 nova, the apparent velocity is  $(1+z) + (0.697 \pm 0.064)z^2$ .  
 A plot of the absolute magnitudes is shown in Figure 5.

### 1210 4.2. X-ray background radiation

1211 Since Giacconi et al. (1962) observed the X-ray back-  
 1212 ground there have been many suggestions made to ex-  
 1213 plain its characteristics. Although much of the unres-  
 1214 olved X-ray emission comes from active galaxies, there  
 1215 is a part of the spectrum between about 10 keV and 1  
 1216 MeV that is not adequately explained by emission from  
 1217 discrete sources. The very high energy range is most

likely due to external point sources. It is the intermediate range that is examined here.

In  $\Lambda$ CDM cosmology for the intermediate X-ray range of about 10–300 keV, the production of X-rays in hot cosmic plasma through the process of bremsstrahlung has been suggested by Hoyle (1962); Gould & Burbidge (1963); Field & Henry (1964); Cowsik & Kobetich (1972).

In a review of the spectrum of the X-ray background radiation Holt (1992) concluded that the measured spectra of discrete sources are not consistent with the observations in the intermediate energy range but there is a remarkable fit to a 40 keV ( $4.6 \times 10^8$  K) bremsstrahlung spectrum from a diffuse hot gas.

However, in an expanding universe most of the X-rays are produced at redshifts of  $z \approx 3$  where the density is large enough to scatter the CMBR. This scattering known as the Sunyaev–Zel’dovich effect (see Section 4.12) makes a distinct change in the spectrum of the CMBR. This predicted change in the spectrum has not been observed and this is the major reason why the bremsstrahlung model in  $\Lambda$ CDM is rejected.

In Curvature-cosmology, the basic component of the universe is plasma with a very high temperature, and with low enough density to avoid the Sunyaev–Zel’dovich effect.

The background X-ray emission is produced in this plasma by the process of free-free emission (bremsstrahlung). The observations of the background X-ray emission are analyzed in order to measure the density and temperature of the plasma. In Curvature-cosmology, this density is the major free parameter and it determines the size of the universe and the value of the Hubble constant.

In addition, the temperature of the plasma determined from the X-ray measurements can be compared with the predicted value from Curvature-cosmology for pure hydrogen of  $2.456 \times 10^9$  K.

The first step is to calculate the expected X-ray emission from high temperature plasma in thermal equilibrium. Here the dominant mechanism is bremsstrahlung radiation from electron-ion and electron-electron collisions. With a temperature  $T$  and emission into the frequency range  $\nu$  to  $\nu + d\nu$  the volume emissivity per steradian can be written as

$$j_\nu(\nu)d\nu = \left(\frac{16}{3}\right) \left(\frac{\pi}{6}\right)^{1/2} r_0^3 m_e c^2 \left(\frac{m_e c^2}{kT}\right)^{1/2} \times g(\nu, T) \exp\left(-\frac{h\nu}{kT}\right) N_e \sum Z_i^2 N_i d\nu, \quad (39)$$

where  $g(\nu, T)$  is the Gaunt factor,  $N_e$  is the electron number density,  $N_i$  is the ion number density and  $r_0$

is the classical electron radius and the other symbols have their usual significance (Nozawa, Itoh, & Kohyama 1998). The intensity,  $j_\nu(\nu)$ , has the units of  $\text{W m}^{-3} \text{Hz}^{-1}$ .

As it stands this equation does not include the electron-electron contribution. Nozawa et al. (1998) and Itoh et al. (2000) have done accurate calculations for many light elements. Based on their calculations Professor Naoki Itoh (<http://www.ph.sophia.ac.jp/>) provides a subroutine to calculate the Gaunt factor that is accurate for temperatures greater than  $3 \times 10^8$  K. It is used here.

Because of the very high temperature, we can assume that all atoms are completely ionized. Thus, Eq. 39 including the Gaunt factor provides the production rate of X-ray photons as a function of the plasma temperature and density.

The next step is to compute the expected intensity at an X-ray detector. Consider an X-ray photon that is produced at a distance  $R\chi$  from the detector. During its travel to the detector, it will have many Curvature-redshift interactions. Although the photon is destroyed in each interaction, there is a secondary photon produced that has the same direction but with a slightly reduced energy.

It is convenient to consider this sequence of photons as a single particle and to refer to it as a primary photon. The important result is that the number of these primary photons is conserved. Therefore, we need the production distribution of the number of photons per unit energy interval. The number of photons emitted per unit volume per unit time in the energy interval  $\varepsilon$  to  $\varepsilon + d\varepsilon$  is given by

$$j_n(\varepsilon) d\varepsilon = \frac{j_\nu(\nu)}{\varepsilon} h d\nu, \quad (40)$$

where  $\varepsilon = h\nu$ ,  $h$  is Planck’s constant and  $j_\nu(\nu)$  is the energy distribution per unit frequency interval.

Now consider the contribution to the number of X-rays observed by a detector with unit area. Because the universe is static, the area at a distance  $R$  from the source is the same as the area at a distance  $R$  from the detector. Since there is conservation of these photons, the number coming from a shell at radius  $R$  per unit time and per steradian within the energy interval  $\varepsilon$  to  $\varepsilon + d\varepsilon$  is

$$\frac{dn(r)}{dt} d\varepsilon = j_n(\varepsilon) d\varepsilon R d\chi.$$

Next, we integrate the photon rate per unit area and per steradian from each shell where the emission energy is  $\varepsilon$  and the received energy is  $\varepsilon_0$  to get

$$I_n(\varepsilon_0) d\varepsilon_0 = R \int_0^{\chi_m} j_n(\varepsilon) d\varepsilon d\chi,$$

1311 where  $\varepsilon = (1+z)\varepsilon_0$  and it is assumed that the flux is  
 1312 uniform over the  $4\pi$  steradian. Furthermore, it is useful  
 1313 to change the independent coordinate to the redshift  
 1314 parameter  $z$ .

1315 Then using Eq. 40 we get

$$I_\nu(\nu_0) d\nu_0 = \frac{c}{H} \int_0^{z_m} \frac{j_\nu(\nu)}{1+z} dz d\nu_0,$$

1316 where  $H$  is the Hubble constant and the change in band-  
 1317 width factor  $d\nu/d\nu_0$ , cancels the  $(1+z)$  factor that comes  
 1318 from the change in variable from  $d\chi$  to  $dz$  but there is  
 1319 another divisor of  $(1+z)$  that accounts for the energy  
 1320 lost by each photon.

1321 Thus the energy flux per unit area, per unit energy  
 1322 interval, per unit frequency and per solid angle is given  
 1323 by Eq. 41 where Plank's constant is included to change  
 1324 the differential from frequency to energy. The  $z_m$  limit  
 1325 of 8.2 comes from the limit of  $\chi \leq \pi$ .

$$\begin{aligned} I_\nu(\nu_0) &= \left(\frac{16}{3}\right) \left(\frac{\pi}{6}\right)^{1/2} \frac{r_0^3 m_e c^3}{h} (8\pi G M_H)^{-1/2} \left(\frac{mc^2}{kT}\right)^{1/2} \\ &\quad \times n_e n_i N_\epsilon^{3/2} \int_0^{z_m} \frac{g((1+z)\nu_0, T)}{(1+z)} \exp\left(-\frac{h(1+z)\nu_0}{kT}\right) dz \\ &= \frac{1.9094 \times 10^3 \text{ keV}}{\text{keV m}^2 \text{ s sr}} \left(\frac{mc^2}{kT}\right)^{1/2} n_e n_i N_\epsilon^{3/2} \\ &\quad \times \varepsilon_0 \int_0^{z_m} \frac{g((1+z)\nu_0, T)}{(1+z)} \exp\left(-\frac{h(1+z)\nu_0}{kT}\right) dz. \end{aligned} \quad (41)$$

1326 The density  $N_\epsilon$  is obtained by fitting Eq. 41 to the  
 1327 observed data as a function of the temperature  $T$ , and  
 1328 then extracting  $N_\epsilon$  from the normalization constant.

1329 The X-ray data used is tabulated in Table 3. It con-  
 1330 sists of the background X-ray data cited in the literature  
 1331 and assessed as being the latest or more accurate results.  
 1332 Preliminary analysis showed that there were some dis-  
 1333 crepant data points that are listed in Table 4 in order of  
 1334 exclusion.

1335 Very hard X-rays cannot be produced even by this hot  
 1336 plasma and are presumably due to discrete sources (Holt  
 1337 1992).

1338 The results of the fit of the data to this model of pure  
 1339 hydrogen is a temperature of

$$(2.62 \pm 0.13) \times 10^9 \text{ K}, \quad (42)$$

1340 which is good agreement with the predicted temperature  
 1341 of  $2.456 \times 10^9$  K.

1342 The measured density is

$$1.93 \pm 0.13 \text{ H atoms per m}^3, \quad (43)$$

**Table 3.** List of background X-ray data used.

Name	Instrument	Reference
Gruber	HEAO 1 A-4	Gruber et al. (1999)
Kinzer	HEAO 1 MED	Kinzer et al. (1997)
Dennis	OSO-5	Dennis et al. (1973)
Mazets	Kosmos 541	Mazets et al. (1975)
Mandrou	Balloon	Mandrou et al. (1979)
Trombka	Apollo 16, 17	Trombka et al. (1977)
Santalogo	Rocket	Santangelo et al. (1973)
Fukada	Rocket	Fukada et al. (1975)

**Table 4.** Background X-ray data: rejected points.

Source	Energy keV	Flux density keV/(keV cm <sup>2</sup> s sr)	$\chi^2$ (1 DoF)
Gruber	98.8	0.230±0.012	108.6
Gruber	119.6	0.216±0.022	65.2
Fukada	110.5	0.219±0.011	66.6
Gruber	152.6	0.140±0.022	50.9
Fukada	179.8	0.110±0.005	41.5
Gruber	63.9	0.484±0.034	25.1

1343 which is the only free parameter in Curvature-  
 1344 cosmology.

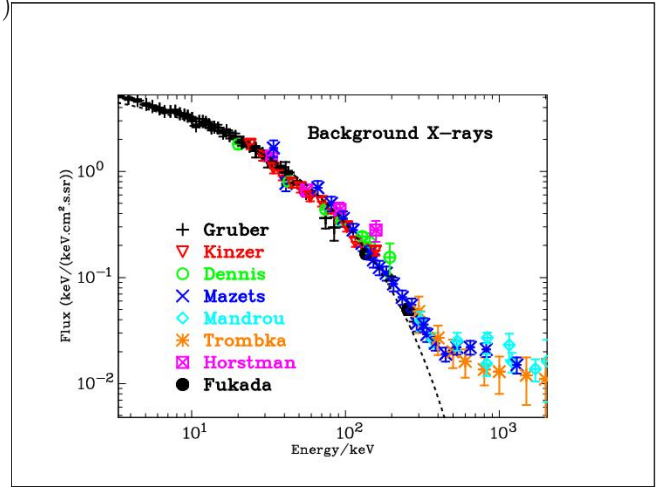


**Figure 6.** Background X-ray spectrum. See Table 3 for list of observations. The dashed (black) line is best fit from 10 keV to 300 keV for the pure hydrogen model.

1345 Most of the X-ray flux below 10 keV and part of the  
 1346 flux just above 10 keV is emission from discrete sources.  
 1347 The deviation from the curve at energies above about  
 1348 300 keV arises from X-rays coming from discrete sources.



In the intermediate region where bremsstrahlung should dominate, there are clear signs of some minor systematic errors. In addition, there appears to be some variation between the data sets. It is not clear whether the discrepancy between the observed points and the predicted flux densities is due to an inadequate theory, inadequate X-ray emission model, or systematic errors in the observations. After all the measurements are very difficult and come from a wide range of rocket, balloon and satellite experiments. In particular, the recent HEAO results [Kinzer et al. \(1997\)](#) differ from earlier results reported by [Marshall et al. \(1980\)](#).

In Curvature-cosmology, the argument against bremsstrahlung based on the Sunyaev–Zel’dovich effect is not valid because the density of the gas is much less and the CMBR has a different source.

#### 4.3. *Cosmic microwave background radiation.*

The cosmic microwave background radiation (CMBR) is one of the major success stories for the standard model. The observed radiation has a spectrum that is extremely close to a black body spectrum which means that it can be described by a single parameter, its temperature.

Observations of the CMBR spectrum were obtained from the FIRAS instrument on the *Cobe* satellite by [Mather et al. \(1990\)](#). They measured the temperature of the CMBR to be 2.725 K. This temperature is in agreement with the observations of [Roth & Meyer \(1995\)](#) who measured a temperature of  $2.729(+0.023, -0.031)$  K using cyanogen excitation in diffuse interstellar clouds. More recently [Fixsen \(2009\)](#) using data from the Wilkinson Microwave Anisotropy Probe (WMAP) and many earlier results provide a temperature of  $2.72548 \pm 0.00057$  K.

The theoretical value from Curvature-cosmology is 2.736 which is within 0.4% but well outside the WMAP uncertainty. However there is a fundamental difference between the two values in that the standard model assumes that the CMBR arose just after the big bang and has been redshifted to its current value. That is the observed value will have radiation from distances with presumed higher redshifts. Whether this can explain the small discrepancy depends on details of the analysis.

#### 4.4. *Tolman surface.*

This test, suggested by [Tolman \(1934\)](#), relies on the observation that the surface brightness of objects does not depend on the geometry of the universe. Although it is obviously true for Euclidean geometry, it is also true for non-Euclidean geometries. For a uniform source, the quantity of light received per unit angular area is independent of distance. However, the quantity of light

is also sensitive to non-geometric effects, which make it an excellent test to distinguish between cosmologies. For expanding universe cosmologies the surface brightness is predicted to vary as  $(1+z)^{-4}$ , where one factor of  $(1+z)$  comes from the decrease in energy of each photon due to the redshift, another factor comes from the decrease in the rate of their arrival and two factors come from the apparent decrease in area due to aberration. This aberration is simply the rate of change of area for a fixed solid angle with redshift. In a static, tired-light, cosmology (such as Curvature-cosmology) only the first factor is present. Thus an appropriate test for Tolman surface brightness is the value of this exponent.

The obvious candidates for surface brightness tests are elliptical and S0 galaxies which have minimal projection effects compared to spiral galaxies. The major problem is that surface brightness measurements are intrinsically difficult due to the strong intensity gradients across their images. In a series of papers [Sandage & Lubin \(2001\)](#); [Lubin & Sandage \(2001a,b,c\)](#) (hereafter SL01) have investigated the Tolman surface brightness test for elliptical and S0 galaxies. More recently [Sandage \(2010\)](#) has done a more comprehensive analysis but since he came to the same conclusion as the earlier papers and since the earlier papers are better known this analysis will concentrate on them.

The observational difficulties are thoroughly discussed by [Sandage & Lubin \(2001\)](#) with the conclusion that the use of Petrosian metric radii helps solve many of the problems. [Petrosian \(1976\)](#); [Djorgovski & Spinrad \(1981\)](#); [Sandage & Perelmuter \(1990\)](#) showed that if the ratio of the average surface brightness within a radius is equal to  $\eta$  times the surface brightness at that radius then that defines the Petrosian metric radius,  $\eta$ . The procedure is to examine an image and to vary the angular radius until the specified Petrosian radius is achieved.

Thus, the aim is to measure the mean surface brightness for each galaxy at the same value of  $\eta$ . The choice of Petrosian radii greatly diminishes the differences in surface brightness due to the luminosity distribution across the galaxies. However, there still is a dependence of the surface brightness on the size of the galaxy which is the Kormendy relationship ([Kormendy 1977](#)).

The purpose of the preliminary analysis done by SL01 is not only to determine the low redshift absolute luminosity but also to determine the surface brightness versus linear size relationship that can be used to correct for effects of size variation in distant galaxies. The data on the nearby galaxies used by SL01 was taken from [Postman & Lauer \(1995\)](#) and consists of extensive data on the brightest cluster galaxies (BCG) from 119



**Table 5.** Galactic properties for Petrosian radius  $\eta = 2.0$

Cluster	$N$	$\overline{\log(S_{BB})}$	$\overline{m_{BB}}$	$\overline{M_{BB}}$
Nearby	74	$4.69 \pm 0.28$	$22.56 \pm 0.84$	$-23.84 \pm 0.66$
1324+3011	11	$3.99 \pm 0.21$	$22.87 \pm 0.75$	$-23.28 \pm 0.65$
1604+4304	6	$4.05 \pm 0.17$	$22.34 \pm 0.60$	$-23.51 \pm 0.68$
1604+4321	13	$4.00 \pm 0.15$	$22.35 \pm 0.78$	$-23.33 \pm 0.64$

**Table 6.** Fitted exponents for distant clusters ( $\eta = 2.0$ )

Cluster	Col	$\bar{z}$	$n_{BB}$	$n_{SL01}$
1324+3011	$I$	0.757	$1.98 \pm 0.19$	$1.99 \pm 0.15$
1604+4304	$I$	0.897	$2.22 \pm 0.22$	$2.29 \pm 0.21$
1604+4321	$R$	0.924	$2.24 \pm 0.18$	$2.48 \pm 0.25$

1451 nearby Abell clusters. All magnitudes for these galaxies  
1452 are in the  $R_C$  (Cape/Landolt) system.

1453 Since the results for different Petrosian radii are highly  
1454 correlated the analysis repeated here using similar pro-  
1455 cedures will use only the Petrosian  $\eta = 2$  radius. Al-  
1456 though the actual value used for  $h$  does not alter any  
1457 significant results here, it is set to  $h = 0.5$  for numeri-  
1458 cal consistency. A minor difference is that the angu-  
1459 lar radius used here is provided by Curvature-cosmology  
1460 whereas they used the older Mattig equation.

1461 The higher  $z$  data also comes from SL01. They made  
1462 Hubble Space Telescope observations of galaxies in three  
1463 clusters and measured their surface brightness and radii.  
1464 The names and redshifts of these clusters are given in  
1465 Table 5 which also shows the number of galaxies in each  
1466 cluster,  $N$ , the logarithm of the average metric radius  
1467 in kpc,  $\log(S_{BB})$ , and the average apparent magnitude  
1468 and the absolute magnitude. In order to avoid confusion  
1469 in  $BB$  denotes a measurement made using the standard  
1470  $\Lambda$ CDM cosmology. Note that the original magnitudes  
1471 for Cl 1324+3011 and Cl 1604+4304 were observed in  
1472 the  $I$  band.

1473 In order to get a reference surface brightness at  $z = 0$   
1474 all the surface brightness values, SB, of the nearby galax-  
1475 ies were reduced to absolute surface brightness by using  
1476 Eq. 44. Since all the redshifts are small, this reduction  
1477 is essentially identical for all cosmological models. How-  
1478 ever the calculation of the metric radii for the distant  
1479 galaxies is very dependent on the cosmological model.

1480 This procedure of using the same cosmology in analyz-  
1481 ing a test of that cosmology is discussed in SL01. Their  
1482 conclusion is that it reduces the significance of a positive  
1483 result from being *strongly supportive* to being *consistent*  
1484 *with the model*. Of interest is that Table 5 shows that on  
1485 average the distant galaxies are fainter than the nearby  
1486 galaxies.

1487 Then a linear least squares fit of the absolute surface  
1488 brightness as a function of  $\log(S_{BB})$ , the Kormendy re-  
1489 lationship, for the nearby galaxies results in the equation

$$SB = 9.29 \pm 0.50 + (2.83 \pm 0.11) \log(S_{BB}) \quad (44)$$

1490 whereas SL01 found the slightly different equation

$$SB = 8.69 \pm 0.06 + (2.97 \pm 0.05) \log(S_{BB}). \quad (45)$$

1491 Although a small part of the discrepancy is due to  
1492 slightly different procedures, the main reason for the  
1493 discrepancy is unknown. Of the 74 galaxies used, there  
1494 were 19 that had extrapolated estimates for either the  
1495 radius or the surface brightness or both. In addition  
1496 there were only three galaxies that differed from the  
1497 straight line by more than  $2\sigma$ . They were A147 ( $2.9\sigma$ ),  
1498 A1016 ( $2.0\sigma$ ) and A3565 ( $-2.4\sigma$ ). Omission of all or some  
1499 of these galaxies did not improve the agreement. The  
1500 importance of this preliminary analysis is that Eq. 44  
1501 contains all the information that is needed from the  
1502 nearby galaxies in order to calibrate the distant clus-  
1503 ter galaxies.

1504 Next we use the galaxies' radius and Eq. 44 to correct  
1505 the apparent surface brightness of the distant galaxies  
1506 for the Kormendy relation and then do least squares fit  
1507 to the difference between the corrected surface bright-  
1508 ness and its absolute surface brightness as a function  
1509 of  $2.5 \log(1+z)$  to estimate the exponent,  $n$ , where  
1510  $SB \propto (1+z)^n$ . If needed the non-linear corrections  
1511 given by Sandage (2010) were applied to the nearby sur-  
1512 face brightness values. For the  $I$  band galaxies, the ab-  
1513 solute surface brightness included the color correction  
1514  $< R - I > = 0.62$  Lubin & Sandage (2001c).

1515 The results for the exponent,  $n$ , for each cluster are  
1516 shown in Table 6 together with the values from SL01  
1517 (column 5) where the second column is the band (color)  
1518 in which the cluster was observed.

1519 Because the definition of magnitude contains a nega-  
1520 tive sign the expected value for  $n$  in BB is four. Nearly  
1521 all of the difference between these results and those from  
1522 SL01 arise from the use of a different Kormendy relation-  
1523 ship. If the Kormendy relationship used by SL01 Eq. 45  
1524 is used instead of Eq. 44) the agreement is excellent. If  
1525 it is assumed that there is no evolutionary or other dif-  
1526 ferences between the three clusters and all the data are  
1527 combined the resulting exponent is  $n_{BB} = 2.16 \pm 0.13$ .

1528 Clearly, there is a highly significant disagreement be-  
1529 tween the observed exponents and the expected expo-  
1530 nent of four. Both SL01 and Sandage (2010) claim that  
1531 the difference is due to the effects of luminosity evolu-

tion. Based on a range of theoretical models SL01 show that the amount of luminosity evolution expressed as the exponent,  $p = 4 - n_{BB}$ , varies between  $p = 0.85$ – $2.36$  in the  $R$  band and  $p = 0.76$ – $2.07$  in the  $I$  band. In conclusion, to their analysis, they assert that *they have either (1) detected the evolutionary brightening directly from the SB observations on the assumption that the Tolman effect exists or (2) confirmed that the Tolman test for the reality of the expansion is positive, provided that the theoretical luminosity correction for evolution is real.*

SL01 also claims that their results are completely inconsistent with a tired light cosmology. Although this is explored for Curvature-cosmology in the next subsection, it is interesting to consider a very simple model. The essential property of a tired light model is that it does not include the time dilation factor of  $(1 + z)$  in its angular radius equation. Thus assuming BB but without the  $(1 + z)$  term all values of  $\log(S_{BB})$  will be increased by  $\log(1 + z)$ . Hence the predicted absolute surface brightness will be (numerically) increased by  $(2.83/2.5)\log(1 + z)$ . For example, the exponent for all clusters will be changed to

$$n_{\text{tired\_light}} = 2.16 \pm 0.16 - \frac{2.83}{2.5} = 1.03 \pm 0.16$$

This is clearly close to the expected value of unity predicted by a tired-light cosmology and thus disagrees with the conclusion of SL01 that the data are incompatible with a tired light cosmology.

There are two major criticisms of this work. The first is that relying on theoretical models to cover a large gap between the expected index and the measured index makes the argument very weak. Although SL01 indirectly consider the effects of relatively common galaxy interactions and mergers in the very wide estimates they provide for the evolution, the fact that there is such a wide spread makes the argument that Tolman surface brightness for this data is consistent with  $\Lambda$ CDM possible but weak.

Ideally, there would be an independent estimate of  $p$  based on other observations. The second criticism is that the nearby galaxies are not the same as the distant cluster galaxies. The nearby galaxies are all brightest cluster galaxies (BCG) whereas the distant cluster galaxies are normal cluster galaxies. It is well known that BCG (Blanton & Moustakas 2009) are in general much brighter and larger than would be expected for the largest member of a normal cluster of galaxies. Whether or not this amounts to a significant variation is unknown but it does violate the basic rule that like should be compared with like.

Unsurprisingly it is found that using Curvature-cosmology the relationship between absolute surface

**Table 7.** Radii and fitted exponents for distant clusters ( $\eta = 2.0$ )

Cluster	$N$	$\log(\bar{S})$	$\bar{M}$	$n$
nearby	74	$4.70 \pm 0.28$	$-23.78 \pm 0.66$	
1324+3011	11	$4.18 \pm 0.21$	$-22.41 \pm 0.66$	$1.19 \pm 0.19$
1604+4304	6	$4.27 \pm 0.17$	$-22.54 \pm 0.65$	$1.45 \pm 0.21$
1604+4321	13	$4.23 \pm 0.15$	$-22.33 \pm 0.68$	$1.48 \pm 0.17$

brightness and radius is identical to that shown in Table 5. What is different is the average radius, the absolute magnitudes and the observed exponent  $n$ . These are shown in Table 7.

The result for all clusters is  $n = 1.38 \pm 0.13$  which is in agreement with unity. Note that the critical difference from the standard analysis is in the size of the radii. They are not only much closer to the nearby galaxy radii but because they are larger they do not require the non-linear corrections for the Kormendy relation. As before we note that the nearby galaxies are BCG which may have a brighter SB than the normal field galaxies. If this is true, it would bias the exponent to a larger value. If we assume that Curvature-cosmology is correct then this data shows that on average the BCG galaxies are  $-0.64 \pm 0.08$  mag (which is a factor of 1.8 in luminosity) brighter than the general cluster galaxies.

The SL01 data for the surface brightness of elliptic galaxies is consistent with  $\Lambda$ CDM but only if a large unknown effect of luminosity evolution is included. The data do not support expansion and are in complete agreement with Curvature-cosmology.

#### 4.5. Dark matter and Coma cluster

All observational evidence for dark matter comes from the application of Newtonian gravitational physics to either clusters of objects or the rotation of galaxies. Galaxy rotation will be dealt with in Section 4.20. The original concept for dark matter comes from applying the virial theorem to the Coma cluster of galaxies (Zwicky 1937). The virial theorem is a statistical theorem that states that for an inverse square law the average kinetic energy of a bound system is equal to half the potential energy (i.e.  $2T + V = 0$ ).

Then with knowing the linear size of the cluster and measuring the mean square spread of velocities we can estimate the total mass of the cluster. There is no doubt that applying the virial theorem to the Coma and other clusters of galaxies provides mass estimates that can be several hundred times the mass expected from the total luminosity. Even the mass of intergalactic gas is not enough to overcome this imbalance. In  $\Lambda$ CDM cosmology

ogy dark matter has been introduced to make up for the shortfall of mass.

However if Curvature-cosmology is valid then it is possible that the observed redshifts are not due to kinematic velocities but are Curvature-redshifts produced by the intergalactic gas. The purpose of this section is to show that Curvature-redshift can explain the galactic velocities without requiring dark matter.

For simplicity, we will use the Coma cluster as a test bed. Not only is it very well studied, but it also has a high degree of symmetry and the presence of an intergalactic gas cloud is known from X-ray observations. [Watt et al. \(1992\)](#) and [Hughes \(1989\)](#) have fitted the density of the gas cloud to an isothermal model with the form

$$\rho = \rho_0 \left( 1 + \left( \frac{r}{r_e} \right) \right)^{-\alpha}, \quad (46)$$

with a center at  $12^h59^m10^s, 27^\circ59'56''$  (J2000) and with  $r_e = 8.8' \pm 0.7', \alpha = 1.37 \pm 0.09, \rho_0 = (2.67 \pm 0.22) \times 10^3 N_e$ . The central density is obtained from the X-ray luminosity and has a strong dependence on the distance. [Watt et al. \(1992\)](#) assumed a Hubble constant of  $50 \text{ km s}^{-1} \text{ Mpc}^{-1}$ . With a mean velocity of  $6,853 \text{ km s}^{-1}$  ([Colless & Dunn 1996](#)) and with this Hubble constant, the distance to the Coma cluster is 137 Mpc. Recently [Rood \(1988\)](#) using the Tully–Fisher relation to measure the distance modulus to the galaxies in the Coma cluster, to observe a value of  $34.4 \pm 0.2$  mag whereas [Liu & Graham \(2001\)](#) using infrared surface brightness fluctuations get  $34.99 \pm 0.21$  mag. The average is 34.7 mag that corresponds to a distance of 87.1 Mpc. This is consistent with the distance of 85.6 Mpc given by [Freedman et al. \(2001\)](#).

The galactic velocity data are taken from [Beijersbergen \(2003\)](#) who provide information for 583 galaxies. The velocity centroid of the Coma cluster is  $12^h59^m19^s, 27^\circ52'2''$  (J2000). They find that early-type galaxies (E+S0+E/S0) have a mean velocity of  $9,926 \text{ km s}^{-1}$  and a rms (root-mean-square) velocity, of  $893 \text{ km s}^{-1}$ . Let us assume that all the galactic velocities are due to Curvature-redshift. That is we assume that the actual velocities, the peculiar velocities, are negligible. Then the redshifts for the galaxies are calculated (in velocity units) by

$$v = v_0 + \int_0^Z 51.691 \sqrt{N(Z)} dZ \text{ km s}^{-1}, \quad (47)$$

where  $Z$  is the distance from the central plane of the Coma cluster to the galaxy measured in Mpc,  $N(Z)$  is the density of the intergalactic gas cloud and  $v_0$  is the average velocity of the galaxies in the cluster. The problem here is that we do not know  $Z$  distances. Nevertheless,

**Table 8.** Coma velocity dispersions for some distances.

Distance/Mpc	50	87	100	150
Dispersion / $\text{km s}^{-1}$	318	554	636	955

we can still get a good estimate by assuming that the distribution in  $Z$  is statistically identical to that in  $X$  and in  $Y$ . In a Monte Carlo simulation, each galaxy was given a  $Z$  distance that was the same as the  $X$  (or  $Y$ ) distance of one of the other galaxies in the sample chosen at random. For 50 trials, the computed dispersion was  $554 \text{ km s}^{-1}$  which can be compared with the measured dispersion of  $893 \text{ km s}^{-1}$ . Curvature-cosmology has predicted the observed dispersion of galactic velocities in the Coma cluster to within a factor of two.

Considering that this is a prediction of the cosmological model without fitting any parameters and ignoring all the complications of the structure both in the gas and galactic distributions the agreement is remarkable.

Since the distance to the Coma cluster is an important variable, the computed velocity dispersion from the Monte Carlo simulation for some different distances (all the other parameters are the same) is shown in [Table 8](#). Thus, the redshift dispersion (in velocity units) is approximately a linear function of the Coma distance. This is not surprising since in this context the distance is mainly a scale factor.

[Beijersbergen \(2003\)](#) note that a better fit to the velocity distribution is provided by the sum of two Gaussian curves. Their best fit parameters for these two Gaussians are  $v_1 = 7,501 \pm 187 \text{ km s}^{-1}$ , with  $\sigma_1 = 650 \pm 216 \text{ km s}^{-1}$  and  $v_2 = 6641 \pm 470 \text{ km s}^{-1}$ , with  $\sigma_2 = 1,004 \pm 120 \text{ km s}^{-1}$ . This double structure is supported by [Colless & Dunn \(1996\)](#) who argue for an ongoing merger between two sub clusters centered in projection on the dominant galaxies NGC 4874 and NGC 4889.

In addition, [Briel, Henry, & Boehringer \(1992\)](#) found evidence for substructure in the X-ray emission and [Finoguenov et al. \(2004\)](#) and [White, Briel, & Henry \(1993\)](#) have measured the X-ray luminosity of individual galaxies in the Coma cluster showing that the model for the gas used above is too simple. The net effect of this substructure is that the observed velocity dispersion would be different from that predicted by a simple symmetric model. Thus, it appears that substructure makes it very difficult to achieve a more accurate test of Curvature-cosmology using the Coma cluster.

There is an important difference between Curvature-redshift and models that assume that the redshifts of the galaxies within a cluster are due to their velocities. Since the laws of celestial mechanics are symmetric in time,

any galaxy could equally likely be going in the opposite direction. Thus a galaxy with a high relative ( $Z$ ) velocity could be in the near side of the cluster or equally likely on the far side of the cluster. However, if the redshifts are determined by Curvature-redshift then there will be a strong correlation in that the higher redshifts will come from galaxies on the far side of the cluster.

A possible test is to see if the apparent magnitudes are a function of relative redshift. With a distance of 87.1 Mpc the required change in magnitude is about  $0.025 \text{ mag Mpc}^{-1}$ . A simple regression between magnitude of Coma galaxies (each relative to its type average) and velocity did not show any significant dependence.

Although this was disappointing, several factors can explain the null result. The first is the presence of the substructure; the second is that the magnitudes for a given galactic type have a standard deviation of about one magnitude, which in itself is sufficient to wash out the predicted effect; and thirdly mistyping will produce erroneous magnitudes due to the different average velocities of different types. In support of the second factor, we note that for 335 galaxies with known types and magnitudes, the standard deviation of the magnitude is 1.08 mag and if we assume that the variance of the  $Z$  distribution is equal to the average of the variances for the  $X$  and  $Y$  distributions then the expected standard deviation of the slope is  $0.076 \text{ mag Mpc}^{-1}$ . Clearly, this is such larger than the expected result of  $0.025 \text{ mag Mpc}^{-1}$ . It is expected that better measurements or new techniques of measuring differential distances will in the future make this a very important cosmological test.

In  $\Lambda$ CDM observations of the velocity dispersion of clusters of galaxies cannot be explained without invoking an ad hoc premise such as dark matter. However Curvature-cosmology not only explains the observations but also makes a good prediction, without any free parameters, of its numerical value.

#### 4.6. Angular size

Closely related to surface brightness is relationship between the observed angular size of a distant object and its actual linear transverse size.

The major distinction in angular size is that Curvature-cosmology, like all tired-light cosmologies, does not include the  $(1+z)$  aberration factor. Its relationship between the observed angular size and the linear size is very close (for small redshifts) to the Euclidean equation.

Gurvits, Kellermann, & Frey (1999) provide a comprehensive history of studies for a wide range of objects that generally show a  $1/z$  or Euclidean dependence. Most observers suggest that the probable cause is some form of

size evolution. Recently López-Corredoira (2010) used 393 galaxies with redshift range of  $0.2 < z < 3.2$  in order to test many cosmologies.

Briefly, his conclusions are

- : *The average angular size of galaxies is approximately proportional to  $z^{-\alpha}$  with  $\alpha$  between 0.7 and 1.2.*
- : *Any model of an expanding universe without evolution is totally unable to fit the angular size data ...*
- : *Static Euclidean models with a linear Hubble law or simple tired-light fit the shape of the angular size vs  $z$  dependence very well: there is a difference in amplitude of 20%–30%, which is within the possible systematic errors.*
- : *It is also remarkable that the explanation of the test results with an expanding model require four coincidences:*
  1. *The combination of expansion and (very strong evolution) size evolution gives nearly the same result as a static Euclidean universe with a linear Hubble law:  $\theta \propto z^{-1}$ .*
  2. *This hypothetical evolution in size for galaxies is the same in normal galaxies as in quasars, as in radio galaxies, as in first ranked cluster galaxies, as the separation among bright galaxies in cluster*
  3. *The concordance model gives approximately the same (differences of less than 0.2 mag within  $z < 4.5$ ) distance modulus in a Hubble diagram as the static Euclidean universe with a linear law.*
  4. *The combination of expansion, (very strong) size evolution, and dark matter ratio variation gives the same result for the velocity dispersion in elliptical galaxies (the result is that it is nearly constant with  $z$ ) as for a simple static model with no evolution in size and no dark matter ratio variation.*

With a redshift range of  $z < 3$  the value of  $S$  is approximately proportional to  $z^{0.68}$  which shows that it is consistent with these results. A full analysis requires a fairly complicated procedure to correct the observed sizes for variations in the absolute luminosity.

A simple example of the angular size test can be done using double-lobed quasars. Using quasar catalogues, Buchalter et al. (1998) carefully selected 103 edge-brightened, double-lobed sources from the VLA FIRST survey and measured their angular sizes directly from the FIRST radio maps.



1816 Since Buchalter et al. (1998) claim that three different  
 1817 Friedmann  $\Lambda$ CDM models fit the data well but that a  
 1818 Euclidean model had a relatively poor fit a reanalysis is  
 1819 warranted.

1820 Their angular sizes were converted to linear sizes for  
 1821 each cosmology and were divided into six bins so that  
 1822 there were 17 quasars in each bin. Because these double-  
 1823 lobed sources are essentially one-dimensional a major  
 1824 part of their variation in size is due to projection effects.

1825 For the moment assume that in each bin they have  
 1826 the same size,  $\hat{S}$ , and the only variation is due to pro-  
 1827 jection then the observed size is  $\hat{S} \sin(\theta)$  where  $\theta$  is the  
 1828 projection angle. Clearly, we do not know the projec-  
 1829 tion angle but we can assume that all angles are equally  
 1830 likely so that if the  $N$  sources, in each bin, are sorted  
 1831 into increasing size the  $i$ 'th source in this list should  
 1832 have, on average, an angle  $\theta_i = \pi(2i - 1)/4N$ . Thus the  
 1833 maximum likelihood estimate of  $\hat{S}$  is

$$\hat{S}_{\text{est}} = \frac{\sum_{i=1}^N \sin(\theta_i) S_i}{\sum_{i=1}^N \sin^2(\theta_i)}.$$

1834 Note that the sum in the denominator is a constant  
 1835 and that the common procedure of using median values  
 1836 is the same as using only the central term in the sum.

1837 Next a regression was done between logarithm of the  
 1838 estimated linear size in each bin and  $\log(1 + z)$  where  $z$   
 1839 is the mean redshift. Then the significance of the test  
 1840 was how close was the exponent,  $b$ , to zero. For  $\Lambda$ CDM  
 1841 the exponent was  $b = -0.79 \pm 0.44$  and for Curvature-  
 1842 cosmology, it was  $b = 0.16 \pm 0.44$ . Although the large  
 1843 uncertainties show that this is not a decisive discrim-  
 1844 ination between the two cosmologies the slope for the  
 1845 Curvature-cosmology suggests that no expansion is more  
 1846 likely.

1847 For angular size the conclusion is in favor of  
 1848 Curvature-cosmology.

#### 1849 4.7. Galaxy distribution

1850 Recently, large telescopes with wide fields and the  
 1851 use of many filters have enabled a new type of galac-  
 1852 tic survey. The light-collecting capability of the large  
 1853 telescopes enables deep surveys to apparent magnitudes  
 1854 of 24 mag or better and the wide field provides a fast  
 1855 survey over large areas.

1856 A major innovation is the use of many filters whose  
 1857 response can be used to classify the objects with great  
 1858 accuracy. Thus, galaxies can be separated from quasars  
 1859 without needing morphological analysis. This photo-  
 1860 metric method of analysis works because photometric  
 1861 templates are available for a wide range of types of galax-  
 1862 ies and other types of objects. In addition, accurate  
 1863 redshifts are obtained from fitting the templates with-

1864 out the tedious procedure of measuring the spectrum of  
 1865 each object.

1866 A typical example of this photometric method is the  
 1867 COMBO-17 survey (Classifying Objects by Medium-  
 1868 Band Observations in 17 filters) provided by Wolf et al.  
 1869 (2004). The goal of this survey was to provide a sample  
 1870 of 50,000 galaxies and 1000 quasars with rather precise  
 1871 photometric redshifts based on 17 colors.

1872 In practice, such a filter set provides a redshift accu-  
 1873 racy of 0.03 for galaxies and 0.1 for quasars. The  
 1874 central wavelength of the 17 filters varied from 364  
 1875 nm to 914 nm and consisted of 5 broadband filters  
 1876 ( $U, B, V, R, I$ ) and 12 narrower-band filters. Wolf et al.  
 1877 (2003) have analyzed this data and claim that there is  
 1878 strong evolution for  $0.2 < z < 1.2$ .

1879 Instead of using generic K-corrections, the intrinsic  
 1880 (rest frame) luminosity of all galaxies are individually  
 1881 measured from their 17-filter spectrum. For each galaxy,  
 1882 three rest-frame pass bands are considered, (i) the SDSS  
 1883  $r$ -band, (ii) the Johnston  $B$ -band and (iii) a synthetic  
 1884 UV continuum band centered at  $\lambda_{\text{rest}} = 280$  nm with 40  
 1885 nm FWHM and rectangular transmission function.

1886 A spectral energy distribution, SED, was determined  
 1887 for each galaxy by template matching. For the evolution  
 1888 analysis, they were assigned to one of four types. The  
 1889 only type that showed a well-defined peak in their lu-  
 1890 minosity distribution was Type 1 which covers the E-S<sub>a</sub>  
 1891 galactic types. The characteristics of the luminosity dis-  
 1892 tribution were obtained by fitting a Schechter function  
 1893 which is

$$\phi(L) dL \phi^*(L/L^*)^\alpha e^{L/L^*} dL$$

1894 where the luminosity  $L^*$  (and its magnitude  $M^*$ ) is a  
 1895 measure of location and  $\alpha$  is a measure of shape.

1896 They found that a fixed value for  $\alpha$  works quite well  
 1897 for the luminosity functions of individual SED types.  
 1898 Examination of their estimate of  $M^*$  for Type 1 galax-  
 1899 ies showed that if they were converted to Curvature-  
 1900 cosmology magnitudes they were independent of red-  
 1901 shift. This is shown in Table 9 where the data are taken  
 1902 from the appendix to Wolf et al. (2003). The second  
 1903 column is the difference,  $\Delta\mu = \mu_{CC} - \mu_{BB}$ , between BB  
 1904 and CC, (Curvature-cosmology), distance moduli. The  
 1905 remaining columns show the CC absolute magnitudes  
 1906 for the three rest-frame bands.

1907 The last row shows the  $\chi^2$  for the five magnitudes  
 1908 relative to their mean using the given uncertainties (all  
 1909 in the range 0.14-0.23).

1910 With four degrees of freedom, the first two bands show  
 1911 excellent agreement with a constant value. The values  
 1912 for  $M_{280}^*$  have less than a 2.5% chance of being constant.  
 1913 However since most of the discrepancy comes from the  
 1914  $z = 0.3$  value of -17.38 mag and most of this band at



**Table 9.**  $M_{CC}^*$  for SED Type 1 galaxy luminosity distributions.

$z$	$\Delta\mu$	$M_r^{*a}$	$M_B^*$	$M_{280}^*$
0.3	0.426	-20.49	-19.06	-17.38
0.5	0.642	-20.49	-19.15	-17.84
0.7	0.822	-20.77	-19.37	-17.62
0.9	0.975	-20.54	-19.09	-17.79
1.1	1.107	-20.87	-19.23	-18.23
$\chi^2$		3.70	2.32	12.81

<sup>a</sup> Absolute magnitude for the SDSS  $r$ -band

small redshifts is outside the range of the 17 filters this discrepancy can be ignored.

If this value is ignored, the  $\chi^2$  is reduced from 12.81 to 6.12 (with 3 DOF) which is consistent with being constant. Since  $\alpha$  is independent of redshift, the result is that if the data had been analyzed using Curvature-cosmology the magnitude for these Type 1 galaxies does not vary with redshift.

Thus we have the surprising result that using  $\Lambda$ CDM a class of galaxies has a well-defined luminosity evolution that can be explained by Curvature-cosmology. In other words, there is no expansion.

#### 4.8. Quasar variability in time

One of the major differences between a tired-light cosmology and an expanding universe cosmology is that any expanding universe cosmology predicts that time variations and clocks have the same dependence on redshift as does the frequency of the radiation.

Hawkins (2010, 2003) has analyzed the variability of 800 quasars covering epoch scales from 50 days to 28 years. His data permitted the straightforward use of Fourier analysis to measure the time scale of the variability. He showed that there was no significant change in the time scale of the variability with increasing redshift. He considered and rejected various explanations including that the time scales of variations were shorter in bluer pass bands or that the variations were not intrinsic but were due to intervening processes such as gravitational micro-lensing. His conclusion was either that the quasars are not at cosmological distances or that the expanding universe cosmologies are incorrect in this prediction.

Curvature-cosmology predicts the observed quasar epoch variability of zero.

#### 4.9. The Butcher-Oemler effect

If there were evidence of significant change in the universe as a function of redshift, it would be a detrimental to any static cosmology. Probably the most important evidence for this cosmic evolution that appears to be in-

dependent of any cosmological model is the Butcher & Oemler (1978) effect. Although the effect has been discussed in earlier papers, the definitive paper is Butcher & Oemler (1984).

They observed that the fraction of blue galaxies in galactic clusters appears to increase with redshift. Clusters allow the study of large numbers of galaxies at a common distance and out to large redshifts, which makes them ideal for studies in evolution. The core regions in a cluster are dominated by early-type (elliptical and lenticular) galaxies, which have a tight correlation between their colors and magnitudes.

We can calculate  $R_{30}$ , the projected cluster-centric radius that contains 30% of the total galaxy population. The blue fraction,  $f_B$ , is defined to be the fraction of galaxies within  $R_{30}$  which are bluer than the color-magnitude relationship for that cluster.

At first sight, this may appear to be a simple test that could be done with apparent magnitudes. However to compare the ratio for distant clusters with that for nearby ones the colors must be measured in the rest frame of each cluster, hence the need to use K-corrections.

The major advantage of the Butcher-Oemler effect is that it is independent of the luminosity-distance relationship that is used. Therefore, to be more precise  $f_B$  is the fraction that has an absolute magnitude  $M_V$ , whose rest frame (B-V) color is at least 0.2 magnitudes bluer than expected. A review by Pimblet (2003) summarizes the important observations.

In its original form the Butcher-Oemler effect is dependent on the apparent magnitude cut-off limits. It is essential that selection effects are the same in the rest frame for each cluster. There are further complications in that the percentage of blue galaxies may or may not depend on the richness of the cluster and the effect of contamination from background galaxies.

Although Pimblet (2003) concluded there was a definite effect, his Fig. 1 shows that this conclusion is open to debate. Since then there have been several attempts to measure an unambiguous effect. Even though they attempted to duplicate the original methodology of Butcher & Oemler, Hawkins (2003) found essentially no effect for K-selected galaxies.

Andreon, Lobo, & Iovino (2004) examined three clusters around  $z=0.7$  and did not find clear-cut evidence for the effect. To quote one of their conclusions: *Twenty years after the original intuition by Butcher & Oemler, we are still in the process of ascertaining the reality of the Butcher-Oemler effect.*

2004 The Butcher-Oemler effect remains uncertain, and  
 2005 therefore does not provide evidence to refute a static  
 2006 cosmology.

2007 4.10. *Fluctuations in the CMBR*

2008 In the model proposed for Curvature-cosmology these  
 2009 fluctuations will also occur but in this case they are due  
 2010 to variations in the density of the cosmic plasma. The  
 2011 CMBR seen through the denser gas within a galactic  
 2012 cluster will have lower than average temperature. [Cabr e  
 2013 et al. \(2006\)](#) show some support for this model in that  
 2014 they have correlated data from the Wilkinson Microwave  
 2015 Anisotropy Probe (WMAP) with galaxy samples from  
 2016 the SDSS DR4 galaxy survey and found a significant cor-  
 2017 relation for the intensity fluctuations with galaxy den-  
 2018 sity.

2019 4.11. *Pioneer 10 acceleration.*

2020 Precise tracking of the *Pioneer 10/11*, *Galileo* and  
 2021 *Ulysses* spacecraft ([Anderson et al. 2002](#)) have shown  
 2022 an anomalous constant acceleration for *Pioneer 10* with  
 2023 a magnitude  $(8.74 \pm 1.55) \times 10^{-10} \text{ m s}^{-2}$  directed towards  
 2024 the sun.

2025 The only method for monitoring *Pioneer 10* is to mea-  
 2026 sure the frequency shift of the signal returned by an  
 2027 active phase-locked transponder. These frequency mea-  
 2028 surements are then processed using celestial mechanics  
 2029 in order to get the spacecraft trajectory.

2030 The simplicity of this acceleration and its magnitude  
 2031 suggests that *Pioneer 10* could be a suitable candidate  
 2032 for investigating the effects of Curvature-redshift. There  
 2033 is a major problem in that the direction of the accel-  
 2034 eration corresponds to a blue shift whereas Curvature-  
 2035 redshift predicts a redshift.

2036 Nevertheless, we will proceed, guided by the coun-  
 2037 terintuitive observation that a drag force on a satellite  
 2038 actually causes it to speed up. This is because the de-  
 2039 crease in total energy makes the satellite change orbit  
 2040 with a redistribution of kinetic and potential energy.

2041 The crucial point of this analysis is that the only in-  
 2042 formation available that can be used to get the *Pioneer*  
 2043 10 trajectory is Doppler shift radar. There is no direct  
 2044 measurement of distance.

2045 Thus the trajectory is obtained by applying celestial  
 2046 mechanics and requiring that the velocity matches the  
 2047 observed frequency shift. Since the sun produces the  
 2048 dominant acceleration, we can consider that all the other  
 2049 planetary perturbations and know drag effects have been  
 2050 applied to the observations and the required celestial  
 2051 mechanics is to be simple two-body motion.

2052 If the observed velocity (away from the sun) is in-  
 2053 creased by an additional apparent velocity due to

2054 Curvature-redshift the orbit determination program will  
 2055 compensate by assuming that the spacecraft is closer to  
 2056 the sun than its true distance. It will be shown that this  
 2057 distance discrepancy produces an extra apparent accel-  
 2058 eration that is directed towards the sun. The test of this  
 2059 model is whether the densities required by Curvature-  
 2060 redshift agree with the observed densities.

2061 Let the actual velocity of *Pioneer 10* at a distance  $r$ ,  
 2062 be denoted by  $v(r)$ , then since the effect of Curvature-  
 2063 redshift is seen as an additional velocity,  $\Delta v(r)$  where  
 2064 from Eq. 11

$$\Delta v(r) = 2\sqrt{8\pi G} \int_0^r \sqrt{\rho(r)} dr \quad (48)$$

2065 where the factor of 2 allows for the two-way trip and  
 2066 the density at the distance  $r$  from the sun is  $\rho(r)$ . Since  
 2067 *Pioneer 10* has a velocity away from the sun, this redshift  
 2068 shows an increase in the magnitude of its velocity.

2069 We will assume that all the perturbations and any  
 2070 other accelerations that may influence the *Pioneer 10*  
 2071 velocity have been removed as corrections to the ob-  
 2072 served velocity and the remaining velocity,  $v(r)$ , is due  
 2073 to the gravitational attraction of the sun. In this case  
 2074 the energy equation is

$$v(r)^2 = v_\infty^2 + \frac{2\mu}{r}, \quad (49)$$

2075 where  $\mu = GM$  is the gravitational constant times the  
 2076 mass of the sun ( $\mu = 1.327 \times 10^{20} \text{ m}^3 \text{ s}^{-2}$ ) and  $v_\infty$  is the  
 2077 velocity at infinity.

2078 The essence of this argument is that the tracking pro-  
 2079 gram is written to keep energy conserved so that an  
 2080 anomalous change in velocity,  $\Delta v(r)$ , will be interpreted  
 2081 as a change in radial distance which is

$$\Delta r = -\sqrt{\frac{2r^3}{\mu}} \Delta v(r).$$

2082 Thus an increase in magnitude of the velocity will be  
 2083 treated as a decrease in radial distance which, in order to  
 2084 keep the total energy constant, implies an increase in the  
 2085 magnitude of the acceleration. Either by using Newton's  
 2086 gravitational equation or by differentiating Eq. 49 the  
 2087 acceleration  $a(r)$  is given by

$$a(r) = -\frac{\mu}{r^2}. \quad (50)$$

2088 Hence with  $v_\infty = 0$  and therefore  $v(r) = \sqrt{2\mu}/r$  we get

$$\Delta a(r) = \frac{2\mu}{r^3} \Delta r = \sqrt{\frac{8\mu}{r^3}} \Delta r$$

2089 and then to the first order an increase in velocity of  
 2090  $\Delta v(r)$  will produce an apparent decrease in acceleration

of  $\Delta a(r)$ , and

$$\begin{aligned}\Delta a &= 8\sqrt{\pi\mu G} r^{-3/2} \int_0^r \sqrt{\rho(r)} dr \\ &= 16\sqrt{\pi\mu G} r^{-1/2} \langle \sqrt{\rho(r)} \rangle \\ &= 6.90R^{-1/2} \langle \sqrt{\rho(r)} \rangle\end{aligned}$$

where for the last equations we measure the distance in AU so that  $r = 1.496 \times 10^{11}R$  and the angle brackets show an average value.

Now fig. 7 from (Anderson et al. 2002) shows that after about 20 AU the anomalous acceleration is essentially constant. The first step is to get an estimate of the required density and see if is feasible.

Using the observed acceleration of  $a_P = 8.74 \times 10^{-10} \text{ m s}^{-2}$  the required average density for the two-way path is  $1.60 \times 10^{-20} R \text{ kg m}^{-3}$  and for  $R=20$  it is  $3.21 \times 10^{-19} \text{ kg m}^{-3}$ .

The only constituent of the interplanetary medium that approaches this density is dust. One estimate by Le Sergeant D'Hendecourt & Lamy (1980) of the interplanetary dust density at 1 AU is  $1.3 \times 10^{-19} \text{ kg m}^{-3}$  and more recently, Grun et al. (1999) suggests a value of  $10^{-19} \text{ kg m}^{-3}$  which is consistent with their earlier estimate of  $9.6 \times 10^{-20} \text{ kg m}^{-3}$  (Grun, Zook, Fechtig, & Giese 1985).

Although the authors do not provide uncertainties, it is clear that their densities could be in error by a factor of two or more. The main difficulties are the paucity of information and that the observations do not span the complete range of grain sizes.

The meteoroid experiment on board *Pioneer 10* measures the flux of grains with masses larger than  $10^{-10} \text{ g}$ . The results show that after it left the influence of Jupiter the flux (Anderson et al. 2002) was essentially constant (in fact there may be a slight rise) out to a distance of 18 AU.

It is thought that most of the grains are being continuously produced in the Kuiper belt. As the dust orbits evolve inwards due to Poynting-Robertson drag and planetary perturbations, they achieve a roughly constant spatial density. The conclusion is that interplanetary dust could provide the required density to explain the anomalous acceleration by a frequency shift due to Curvature-redshift.

Overall, this analysis has shown that it is possible to explain the acceleration anomaly of *Pioneer 10* but that a more definitive result requires Curvature-redshift to be included in the fitting program and more accurate estimates of the dust density are certainly needed. Subject to the caveat about the dust density, Curvature-redshift could explain the anomaly in the acceleration of *Pioneer 10* (and by inference other spacecraft).

Not only can Curvature-cosmology explain the anomalous Pioneer 10 acceleration, it has a feasible prediction of its value.

#### 4.12. The Sunyaev-Zel'dovich effect

The Sunyaev-Zel'dovich effect (Sunyaev & Zeldovich 1970; Peebles 1993) is the effect of Thompson scattering of background radiation by free electrons in the intervening medium. The technique depends on knowing the spectrum of the background source and then measuring the changes in the spectrum due to the intervening plasma.

In particular, it is the scattering in both angle and frequency of the cosmic microwave background radiation (CMBR) by electrons in the cosmic plasma. Because of the rapidly changing density (like  $(1+z)^3$ ) with redshift this is an important effect in  $\Lambda$ CDM cosmology. The effect is often characterized by the dimensionless Compton  $y$ -parameter, which for a distance  $x$  through non-relativistic thermal plasma with an electron density of  $N_e$  has the value

$$y = \frac{kT_e}{m_e c^2} \sigma_T N_e x = 3.46 \times 10^{-16} N_e T_e x \text{ Mpc}, \quad (51)$$

where  $\sigma_T$  is the Thompson cross-section. An object at redshift  $z$  is at the distance  $x = R\chi = 5.80 \times 10^3 N_e^{1/2} \log(1+z) \text{ Mpc}$ . Hence, using  $T_e = 2.62 \times 10^9 \text{ K}$ ,  $N_e = 1.35 \text{ m}^{-3}$  we get  $y = 9.2 \times 10^{-6} \log(1+z)$ .

Using the CMBR as a source the Sunyaev-Zel'dovich effect has been observed and Mather et al. (1990) report an observed upper limit of  $y = 0.001$ , and more recently Fixsen et al. (1996) report  $y = 1.5 \times 10^{-5}$ .

Using this limit with Eq. 51 shows that there is no effect in Curvature-cosmology if  $z < 4.1$ . Although in Curvature-cosmology the CMBR has a more local origin it is of interest to note that this analysis assumes that each photon has many Compton interactions.

For this electron density, the Compton mean free path is 575 Gpc whereas the distance to  $z = 4.1$  is about 3.7 Gpc which means that a negligible number of the photons will have an interaction with the high temperature electrons.

Furthermore the photon energy distribution for a single interaction has a different spectrum for that for the normal Sunyaev-Zel'dovich effect

(Longair 1991; Sunyaev & Zeldovich 1980). Bielby & Shanks (2007) extend the results of Lieu, Mittaz, & Zhang (2006) to show that not only was the Sunyaev-Zel'dovich effect less than what was expected but that it tendered to disappear as the redshift went from 0.1 to 0.3. The conclusion is that Curvature-cosmology is completely consistent with the experimental observations of

2186 the Sunyaev–Zel’dovich effect on the CMBR. Thus the  
 2187 Sunyaev–Zel’dovich effect is important in standard cos-  
 2188 mology it is not important in Curvature-cosmology.

2189 4.13. *Gravitational lensing.*

2190 There are many gravitational lens where a quasar or  
 2191 distant galaxy has one or more images produced by a  
 2192 nearer lensing galaxy or cluster of galaxies. A set of  
 2193 these lensing systems has been examined in the context  
 2194 of Curvature-cosmology to see if it offers a consistent  
 2195 and possibly simpler explanation. The two important  
 2196 measures are the prediction of the mass of the lensing  
 2197 galaxy and the determination of the Hubble constant  
 2198 from the time delays between variations in the luminos-  
 2199 ity of different images. Since the delay measurement  
 2200 is easily done, all that is needed is to measure the dif-  
 2201 ferent path lengths. This path difference involves both  
 2202 geometric and general relativistic corrections.

2203 One of the remarkable properties of gravitational  
 2204 lenses is that the geometry is completely determined by  
 2205 a two-dimensional lensing potential which can be ex-  
 2206 pressed in terms of a surface density at the position of  
 2207 the lensing galaxy. For thin lenses, any two systems with  
 2208 the same surface density distribution have the same lens  
 2209 effect. Now the usual way to determine the surface den-  
 2210 sity is to measure the widths of spectral lines, assume  
 2211 that the width is due to velocity and then use the virial  
 2212 theorem to obtain the surface density.

2213 However in Curvature-cosmology the widths of spec-  
 2214 tral lines are likely to have a large component due to  
 2215 the effects of Curvature-redshift from dust and gas in  
 2216 the lensing object. Thus the widths are not a reliable  
 2217 measure of area density and this method cannot be used.

2218 4.14. *Lyman-alpha forest*

2219 . The Lyman- $\alpha$  (Ly $\alpha$ ) forest is the large number of  
 2220 absorption lines seen in the spectra of quasars. Most  
 2221 of the lines are due to absorption by clouds of neutral  
 2222 hydrogen in the line of sight to the quasar. Some of  
 2223 the lines are due to other elements or due to Lyman- $\beta$   
 2224 absorption.

2225 Because of the redshift between the absorbing cloud  
 2226 and us, the lines are spread out over a range of wave-  
 2227 lengths. Usually the analysis is confined to lines be-  
 2228 tween the Ly $\alpha$  (at a wavelength of 121.6 nm) and Ly $\beta$   
 2229 (at 102.5 nm). Thus, each quasar provides a relatively  
 2230 narrow spectrum of Ly- $\alpha$  lines at a redshift just less than  
 2231 that for the quasar. Since the advent of spacecraft tele-  
 2232 scopes, in which can observe the ultraviolet lines, and  
 2233 by using many quasars the complete redshift range up  
 2234 to the most distant quasar has been covered. The large  
 2235 redshift range makes the Lyman  $\alpha$  spectra potentially a  
 2236 powerful cosmological tool.

2237 The obvious cosmological observation is the density of  
 2238 lines as a function of redshift but as discussed by Rauch  
 2239 (1998) in an excellent review, there are many important  
 2240 observational problems.

2241 The first, which has now been overcome, is that the  
 2242 spectra must have sufficient resolution to resolve every  
 2243 line. The second is that most lines are very weak and  
 2244 the number of resolved lines can depend greatly on the  
 2245 signal-to-noise ratio. This is accentuated because the  
 2246 steep spectrum for the density of lines as a function of  
 2247 their strength means that a small decrease in the ac-  
 2248 ceptance level can drastically increase the number of  
 2249 observed lines. The third problem is that each quasar  
 2250 only provides a set of lines in a narrow range of redshift  
 2251 and there are considerable difficulties in getting uniform  
 2252 cross-calibrations.

2253 In addition to these problems, it will be shown that  
 2254 Curvature-redshift can have a profound effect on the in-  
 2255 terpretation of the line widths and column densities.

2256 Since in Curvature-cosmology, the distribution of  
 2257 clouds is independent of time or distance the expected  
 2258 density of lines as a function of redshift is

$$\frac{dn}{dz} = \frac{AcN_\epsilon}{H(1+z)}, \quad (52)$$

2259 where  $N_0$  is the volume density and  $A$  is the average  
 2260 area of a cloud. Most observers have fitted a power law  
 2261 with the form  $(1+z)^\gamma$  to the observed line densities  
 2262 with a wide range of results. They vary from  $\gamma = 1.89$   
 2263 to  $\gamma = 5.5$  (Rauch 1998). All of which are inconsistent  
 2264 with the Curvature-cosmology prediction of  $\gamma = -1$ .

2265 In Curvature-cosmology, there is the additional ef-  
 2266 fect that much of the line broadening may be due to  
 2267 Curvature-redshift. Curvature-redshift will be operat-  
 2268 ing within the clouds so that the observed line width  
 2269 will be a combination of the usual Voigt profile and the  
 2270 change in the effective central frequency as the photons  
 2271 pass through the cloud. If the cloud has a density  $\rho(x)$   
 2272 at the point  $x$ , measured along the photon trajectory then  
 2273 the change in frequency from the entering frequency due  
 2274 to Curvature-redshift is

$$\frac{\Delta\nu}{\nu} = \frac{1}{c} \int \sqrt{8\pi G\rho(x)} dx.$$

2275 In units of  $N(x) = \rho(x)/m_H$  this is (with  $N$  in  $m^{-3}$  and  
 2276  $dx$  in kpc)

$$\frac{\Delta\nu}{\nu} = -\frac{\Delta\lambda}{\lambda} = \int 1.724 \times 10^{-7} \sqrt{N(x)} dx.$$

2277 Then the final profile will be the combination of the  
 2278 natural line width, the Doppler width due to tempera-  
 2279 ture, any width due to bulk motions and the Curvature-  
 2280 redshift width. Now assuming pure hydrogen, the hy-  
 2281 drogen column density is given by  $N_H = \int N(x) dx$ .



Although it is unlikely that the line of sight goes through the center of the cloud, it is reasonable to expect a roughly symmetric distribution of gas with a shape similar to a Gaussian. We can define an effective density width by

$$x_w^2 = \int (x - \bar{x})^2 N(x) dx / \int N(x) dx.$$

Also define  $N_0 = N_H/x_w$  and an effective velocity width  $\Delta v = 51.68\eta x_w \sqrt{N_0}$  and where  $\eta$  is a small numeric constant that depends on the exact shape of the density distribution. Eliminating the central density, we get (with  $x_w$  in kpc)

$$\Delta v^2 = 8.656 \times 10^{-17} \eta^2 N_H x_w. \quad (53)$$

For values  $N_H = 10^{19} \text{ m}^{-2}$ ,  $x_w = 1 \text{ kpc}$  and with  $\eta = 1$  we get  $\Delta v = 29 \text{ km s}^{-1}$ .

Since there is a wide variation in column densities and the effective widths are poorly known, it is clear that Curvature-redshift could completely dominate many of the Lyman- $\alpha$  line widths and the others would require a convolution of the Doppler profile with the Curvature-redshift density effect. What is also apparent is that the very broad absorption lines may be due to Curvature-redshift acting in very dense clouds.

Although there is uncertainty about the observed relationship between the line width and the column density, we note that for a fixed effective density width, Eq. 53 predicts a square relationship that may be compared with the exponent of  $2.1 \pm 0.3$  found by [Petini et al. \(1990\)](#). Clearly, there needs to be a complete re-evaluation of profile shapes, column densities, and cloud statistics that allows for the effects of Curvature-cosmology. We must await this analysis to see whether the Lyman- $\alpha$  forest can provide a critical test of Curvature-cosmology.

#### 4.15. Nuclear abundances

One of the successes of  $\Lambda$ CDM cosmology is in its explanation of the primordial abundances of the light elements. Since the proposed Curvature-cosmology is static, there must be another method of getting the ‘primordial’ abundances of light elements. In Curvature-cosmology, the primordial abundance refers to the abundance in the cosmic gas from which the galaxies are formed.

The first point to note is that in Curvature-cosmology the predicted temperature of the cosmic plasma is  $2.465 \times 10^9 \text{ K}$  at which temperature nuclear reactions can proceed.

It is postulated that in Curvature-cosmology there is a continuous recycling of material from the cosmic plasma

to galaxies and stars and then back to the gas. Because of the high temperature, nuclear reactions will take place whereby the more complex nuclei are broken down to hydrogen.

#### 4.16. Galactic rotation curves

One of the most puzzling questions in astronomy is: why does the observed velocity of rotation in spiral galaxies not go to zero towards the edge of the galaxy. Simple Keplerian mechanics suggest that there should be a rapid rise to a maximum and then a decrease in velocity that is inversely proportional to the square root of the radius once nearly all the mass has been passed.

Although the details vary between galaxies, the observations typically show a rapid rise and then an essentially constant tangential velocity as a function of radius out to distances where the velocity cannot be measured due to lack of material. The  $\Lambda$ CDM explanation is that this is due to the gravitational attraction of a halo of dark matter that extends well beyond the galaxy. We examine whether this rotation curve can be explained by Curvature-redshift.

Observations show that our own Galaxy and other spiral galaxies have a gas halo that is larger than the main concentration of stars. It is clear that if the observed redshifts are due to Curvature-redshift acting within this halo, the halo must be asymmetric; otherwise, it could not produce the asymmetric rotation curve.

Now the observed velocities in the flat part of the curves are typically 100 to 200  $\text{km s}^{-1}$ . The first step is to see if Curvature-redshift provides the right magnitude for the velocity. For a gas with an average density of  $N_H$  the predicted redshift (in velocity units) is  $5.17 \times 10^{-2} d \sqrt{N} \text{ km s}^{-1}$  where  $d$  is the distance in kpc. For realistic values of  $d = 10 \text{ kpc}$  and  $N = 1.0 \times 10^5 \text{ m}^{-3}$  the velocity is  $163 \text{ km s}^{-1}$ . Thus, the magnitude is feasible.

Although there could be a natural asymmetry in a particular galaxy, the fact that the flattened rotation curve is seen for most spiral galaxies suggests that there is a common cause for the asymmetry.

A partial explanation is that the halos are rotating more like a solid object and that the observed rotation is genuine.

Another possibility is that the asymmetry could arise from ram pressure. Since most galaxies are moving relative to the cosmic medium, it is expected that there will be an enhanced density towards the leading point of the galaxy. This asymmetric density could produce an apparent velocity gradient across the galaxy that could explain the apparent rotation curve.

2378 Naturally, there would be range of orientations and  
 2379 the apparent velocity gradient must be added to any in-  
 2380 trinsic rotation curve to produce a wide diversity of re-  
 2381 sults. Thus, Curvature-redshift could explain the galac-  
 2382 tic rotation curves if there is an asymmetric distribution  
 2383 of material in the galactic halo.

2384 Both cosmologies have problems with galactic rotation  
 2385 curves.  $\Lambda$ CDM cosmology not only requires dark matter  
 2386 but does not have any definite models for its distribu-  
 2387 tion. Curvature-cosmology has the problem of achieving  
 2388 sufficient asymmetry to mimic a rotation curve.

2389 *4.17. Redshifts in our Galaxy*

2390 In our Galaxy, the Milky Way, there is an interesting  
 2391 prediction. The density of the interstellar ionized gas  
 2392 is high enough to inhibit Curvature-redshift for radio  
 2393 frequencies.

2394 From Eq. 36 it was shown that for wavelengths longer  
 2395 than about  $20.6N_e^{-1/2}$  m the effect of refractive index in  
 2396 fully ionized plasma will inhibit Curvature-redshift. The  
 2397 refractive index of neutral hydrogen is too low to inhibit  
 2398 Curvature-redshift. However, any fully ionized plasma  
 2399 with  $N_e > 10^4 \text{m}^{-3}$  will inhibit Curvature-redshift for  
 2400 the 21 cm hydrogen line. Since the local interstel-  
 2401 lar medium has an electron density of about  $10^5 \text{m}^{-3}$   
 2402 Curvature-redshift will be inhibited for the 21 cm hy-  
 2403 drogen in these local regions.

2404 Thus for sight lines close to the Galactic plane we can  
 2405 assume a similar density and thus a similar inhibition  
 2406 with the result that the observed radio redshifts can be  
 2407 correctly interpreted as genuine velocities. Thus, there  
 2408 is little change needed to the current picture of galac-  
 2409 tic structure and rotation derived from 21 cm redshifts.  
 2410 However, there may be some Curvature-redshift present  
 2411 in sight lines away from the plane and especially in the  
 2412 Galactic halo.

2413 Since optical redshifts have the full effects of  
 2414 Curvature-redshift, it should be possible to find objects  
 2415 with discrepant redshifts where the optical redshift is  
 2416 greater than the radio redshift. The difficulty is that the  
 2417 two types of radiation are produced in radically different  
 2418 environments: the optical in compact high temperature  
 2419 objects, such as stars, and the radio in very low-density  
 2420 cold clouds. In addition, there is the complication that  
 2421 within the galactic plane, optical extinction due to dust  
 2422 limits the optical range to about 1 kpc.

2423 Curvature-redshift may help to explain an old stel-  
 2424 lar mystery. There is a long history provided by Arp  
 2425 (1992) of observations of anomalous redshifts in bright  
 2426 hot stars, which is called the K-term or K-effect.

2427 Allen (1976) states that B<sub>0</sub> stars typically show an  
 2428 excess redshift of  $5.1 \text{ m s}^{-1}$ , A<sub>0</sub> have  $1.4 \text{ km s}^{-1}$  and F<sub>0</sub>

2429 have  $0.3 \text{ km s}^{-1}$ . This can be explained if these stars  
 2430 have a large corona that produces a Curvature-redshift.

2431 It is probably no coincidence that such stars have large  
 2432 stellar winds and mass outflows. In order to see if it is  
 2433 feasible let us consider a simple model for the outflow in  
 2434 which the material has a constant velocity  $v_0$ , and con-  
 2435 servation of matter (Gauss's Law) then requires that the  
 2436 density has inverse square law dependence. Although  
 2437 this is incorrect at small stellar radii, it is a reasonable  
 2438 approximation further from the star.

2439 Then if  $\rho_1$  is the density at some inner radius  $r_1$ , then  
 2440 integration of Eq. 25 out to a radius  $r_2$ , the expected  
 2441 redshift in velocity units is

$$v = \sqrt{\frac{2GM}{v_o}} \log\left(\frac{r_2}{r_1}\right),$$

2442 where  $\dot{M}$  is the observed stellar mass-loss-rate. Then  
 2443 with  $\dot{M}$  in solar masses per year, with  $v$  and  $v_0$  in  $\text{km s}^{-1}$ ,  
 2444 the redshift is

$$v = 91.7 \sqrt{\frac{\dot{M}}{v_o}} \log\left(\frac{r_2}{r_1}\right) \text{ km s}^{-1},$$

2445 With  $\dot{M} = 10^{-5} M_\odot \text{ yr}^{-1}$  Cassinelli (1979),  $v_0 =$   
 2446  $1 \text{ km s}^{-1}$  and  $r_2/r_1 = 10^3$  the predicted redshift (in ve-  
 2447 locity units) is  $2 \text{ km s}^{-1}$  which is in reasonable agreement  
 2448 with the observed K-effects mentioned above.

2449 *4.18. Anomalous redshifts*

2450 Arp (1987); Ratcliffe (2010) have argued that there  
 2451 is strong observational evidence for anomalous redshifts  
 2452 between quasars and galaxies.

2453 Typically if there is a quasar very close to a galaxy  
 2454 with a material bridge or other evidence that suggests  
 2455 that they are associated. Chu et al. (1998) report on  
 2456 five X-ray emitting blue stellar objects located less than  
 2457 12 arcmin from the X-ray Seyfert galaxy NGC 3516.  
 2458 In this case the association is that the objects lie close  
 2459 to a straight line on either side of the galaxy and that  
 2460 their redshifts are proportional to  $\log(\theta)$  where  $\theta$  is the  
 2461 angular distance from the central galaxy.

2462 Furthermore the line of objects is within a few degrees  
 2463 of the minor axis of NGC 3516. The measured redshifts  
 2464 are 0.33, 0.69, 0.93, 1.4 and 2.1. NGC 3516 is a barred  
 2465 spiral galaxy and it has a redshift of 0.00884.

2466 Can Curvature-cosmology explain this redshift  
 2467 anomaly? If the objects are seen through a large dense  
 2468 cloud, such as a galactic halo, then Curvature-redshift  
 2469 will produce an extra redshift due to the photons pas-  
 2470 sage through the cloud. the extra redshift,  $\delta$ , is

$$\delta = 1.72 \times 10^{-10} \int \sqrt{N(x)} dx,$$

2471 where  $N(x)$  is the number density and distances are  
 2472 measured in pc. If  $z$  is the cosmological redshift then  
 2473 the extra-observed redshift is  $\Delta z = (1+z)(e^\delta - 1)$ .

2474 In order to achieve an extra redshift  $\delta \approx 1$  with a  
 2475 distance of  $10^4$  pc the gas number density must be about  
 2476  $3 \times 10^{11} \text{ m}^{-3}$ . Now although cold interstellar molecular  
 2477 clouds can have densities reaching this value it is still a  
 2478 very high density.

2479 But if the size is increased by a factor of two, the re-  
 2480 quired density is decreased by a factor of four. Moreover  
 2481 the objects with the largest redshifts are the further-  
 2482 most away from the galaxy. These redshifts could be  
 2483 explained by Curvature- redshift in a very large, very  
 2484 dense galactic halo with a hole in the middle.

2485 Since NGC 3516 has a very low redshift and is seen  
 2486 nearly face on, the implication is that this gas cloud is  
 2487 probably shaped like a torus and it lies in the galactic  
 2488 plane of NGC3516. A further test is to compare an  
 2489 estimate of the mass of this torus with that for a typical  
 2490 galaxy. Since a torus formed by the rotation of a circle  
 2491 with radius  $r$  about a axis in the plane of the circle where  
 2492 the radius of rotation is  $R$ , its volume is  $V = 2\pi^2 Rr^2$ .  
 2493 With  $R$  and  $r$  in kpc and an average density of  $N$  its  
 2494 mass is  $M = 0.484Rr^2N M_{sun}$ . Then with  $R = 15$  kpc,  
 2495  $r = 10$  kpc and  $N = 3 \times 10^{11}$  the mass is  $2 \times 10^{14} M_{sun}$   
 2496 which considerably larger than a normal galaxy.

2497 Since these anomalous redshifts are completely outside  
 2498 any standard cosmological model, the only reason that  
 2499 these observations are not fatal to standard cosmological  
 2500 is their controversial nature.

#### 2501 4.19. Voids

2502 If Curvature-cosmology is valid then the redshift of  
 2503 the galaxies in the Coma cluster (Section 4.5) will have  
 2504 been increased, on average, by the additional redshift  
 2505 due to the intergalactic gas. Thus, they will have, on  
 2506 average, a larger redshift than an isolated galaxy at the  
 2507 same distance.

2508 Table 10 shows the predicted (effective) velocity for  
 2509 a galaxy in the center plane of the Coma cluster as a  
 2510 function of the projected radius. The second column  
 2511 is the velocity at that exact radius and the third col-  
 2512 umn shows the average velocity of galaxies (uniformly  
 2513 spread in area) within that radius. This simulation also  
 2514 showed that the average velocity offset for the galaxies  
 2515 in the Coma cluster is  $1206 \text{ kms}^{-1}$  which means that  
 2516 the redshift of the center of the Coma cluster is  $6926-$   
 2517  $1206=5720 \text{ kms}^{-1}$ . This offset is important for calcu-  
 2518 lating the Hubble constant which from these figures is  
 2519  $5270/87.1=65.7 \text{ kms}^{-1} \text{ Mpc}^{-1}$ .

**Table 10.** Velocity at, and average velocity within various  
 projected radii in the Coma cluster (distance = 87.1 Mpc).

Radius <sup>a</sup> /Mpc	Velocity /km s <sup>-1</sup>	Mean velocity /km s <sup>-1</sup>
0.0	2327.7	2327.7
0.5	1477.7	1764.8
1.0	1033.4	1342.5
1.5	803.3	1096.9
2.0	658.6	933.2
2.5	557.0	814.4
3.0	481.0	723.3
3.5	421.7	650.7
4.0	374.0	541.2
4.5	334.8	541.2
5.0	302.0	498.7

<sup>a</sup> projected radius

2520 In addition, the redshift of objects seen through a clus-  
 2521 ter will be increased by Curvature-redshift from the in-  
 2522 tergalactic gas.

2523 [Karoji, Nottale, & Vigier \(1976\)](#) claim to have seen  
 2524 this effect. They examined radio galaxies and classified  
 2525 them into region A if their light does not pass through  
 2526 a cluster and region B if their light passes through a  
 2527 cluster. They found no significant differences in mag-  
 2528 nitudes between the two regions but they did find a  
 2529 significant difference in the average redshift that was  
 2530 consistent over the complete range.

2531 Their result is that radio galaxies seen through a clus-  
 2532 ter had an average extra redshift (in velocity units) of  
 2533  $2412 \pm 1327 \text{ km s}^{-1}$ . Overall the difference in the dis-  
 2534 tance modulus was  $\mu = 0.16 \pm 0.04$ , which is just signif-  
 2535 icant.

2536 Since the density and distribution of the gas in the  
 2537 clusters is unknown and the limiting radius of the clus-  
 2538 ter is not stated, it is impossible to get an accurate pre-  
 2539 diction.

2540 Nevertheless, we note that for the Coma cluster with  
 2541 a radius of 2 Mpc the average extra redshift (from Ta-  
 2542 ble 10 with a factor of two) corresponds to  $1866 \text{ km s}^{-1}$   
 2543 showing that Curvature-cosmology could explain the ef-  
 2544 fect.

2545 In a different study, [Nottale \(1976\)](#) and [Nottale &  
 2546 Vigier \(1977\)](#) compared the magnitude of the brightest  
 2547 galaxy in a cluster with that in another cluster with  
 2548 similar redshift. They found that there was no signifi-  
 2549 cant difference in magnitudes between clusters but that  
 2550 the clusters with the largest number of galaxies had the  
 2551 higher redshift difference between the pairs.

2552 On average the redshift difference (in velocity units) 2603  
 2553 was  $292 \pm 85 \text{ km s}^{-1}$ . This can be explained by the ex- 2604  
 2554 pected correlation between the number of galaxies and 2605  
 2555 size and density of the intergalactic gas. However it 2606  
 2556 should be noted that these observations have been dis- 2607  
 2557 puted by Rood & Struble (1982). 2608

2558 In his review of voids in the distribution of galax- 2609  
 2559 ies, Rood (1988) quotes Mayall (1960) who observed a 2610  
 2560 large void in the distribution of galaxies in front of the 2611  
 2561 Coma cluster. This void has a magnitude of about 3000 2612  
 2562  $\text{km s}^{-1}$ , which although somewhat larger, is not incon- 2613  
 2563 sistent with the expected value of about  $1200 \text{ km s}^{-1}$ . 2614

2564 In other words, the Coma cluster galaxies have an 2615  
 2565 extra Curvature-redshift due to the intergalactic gas. 2616  
 2566 However, the galaxies just outside the cluster nearer to 2617  
 2567 us do not have this extra redshift and would appear to 2618  
 2568 be closer to us. Hence, we see an apparent void in the 2619  
 2569 redshift distribution in front of the Coma cluster. 2620

2570 A consequence of gas clouds and Curvature-redshift 2621  
 2571 is that the distribution of redshifts is similar to but not 2622  
 2572 identical to the distribution of  $z$  distances. Galaxies that 2623  
 2573 are behind a cloud will have a higher redshift than would 2624  
 2574 be expected from a simple redshift distance relationship. 2625

2575 Thus, we would expect to see anomalous voids and 2626  
 2576 enhancements in the redshift distribution. This will be 2627  
 2577 accentuated if the gas clouds have a higher than average 2628  
 2578 density of galaxies. 2629

2579 de Lapparent et al. (1986) show a redshift plot for a 2630  
 2580 region of the sky that includes the Coma cluster. Their 2631  
 2581 data are from the Center for Astrophysics redshift sur- 2632  
 2582 vey and their plot clearly shows several voids. They 2633  
 2583 suggest that the galaxies are distributed on the surfaces 2634  
 2584 of shells. However, this distribution could also arise from 2635  
 2585 the effects of Curvature-redshift in clouds of gas. 2636

4.20. Entropy

2586  
 2587 Consider a stellar cluster or an isolated cloud of gas 2637  
 2588 in which collisions are negligible or elastic. In either 2638  
 2589 case the virial theorem states that the average kinetic 2639  
 2590 energy  $K$ , is related to the average potential energy  $V$ , 2640  
 2591 by the equation  $V = V_0 - 2K$  where  $V_0$  is the poten- 2641  
 2592 tial energy when there is zero kinetic energy. Let  $U$  be 2642  
 2593 the total energy then  $U = K + V = V_0 - K$ . Thus, 2643  
 2594 we get the somewhat paradoxical situation that since 2644  
 2595  $V_0$  is constant; an increase in total energy can cause a 2645  
 2596 decrease in kinetic energy. This happens because the av- 2646  
 2597 erage potential energy has increased by approximately 2647  
 2598 twice as much as the loss in kinetic energy. Since the 2648  
 2599 temperature is proportional to (or at the least a mono- 2649  
 2600 tonic increasing function of) the average kinetic energy, 2650  
 2601 it is apparent that an increase in total energy leads to a 2651  
 2602 decrease in temperature. This explains the often-quoted 2652

2603 remark that a self-gravitationally bound gas cloud has 2604  
 2605 a negative specific heat capacity. Thus, when gravity 2606  
 2607 is involved the whole construct of thermodynamics and 2608  
 2609 entropy needs to be reconsidered. 2610

2611 One of the common statements of the second law of 2612  
 2613 thermodynamics is that (Longair 1991): *The energy of 2614*  
 2614 *the universe is Constant: the entropy of the Universe 2615*  
 2615 *tends to a maximum, (Feynman 1965): the entropy of 2616*  
 2616 *the universe is always increasing* or from Wikipedia *the 2617*  
 2617 *second law of thermodynamics is an expression of the 2618*  
 2618 *universal law of increasing entropy, stating that the en- 2619*  
 2619 *tropy of an isolated system which is not in equilibrium 2620*  
 2620 *will tend to increase over time, approaching a maximum 2621*  
 2621 *value at equilibrium.* 2622

2623 Now the normal proof of the second law considers the 2624  
 2625 operation of reversible and non-reversible heat engines 2626  
 2626 working between two or more heat reservoirs. If we use a 2627  
 2627 self-gravitating gas cloud as a heat reservoir then we will 2628  
 2628 get quite different results since the extraction of energy 2629  
 2629 from it will lead to an increase in its temperature. Thus 2630  
 2630 if the universe is dominated by gravity the second law 2631  
 2631 of thermodynamics needs reconsideration. In addition, 2632  
 2632 it should be noted that we cannot have a shield that 2633  
 2633 hides gravity. To put it another way there is no adia- 2634  
 2634 batic container that is beyond the influence of external 2635  
 2635 gravitational fields. Thus we cannot have an isolated 2636  
 2636 system. 2637

2638 This discussion shows that in a static finite universe 2639  
 2639 dominated by gravity simple discussions of the second 2640  
 2640 law of thermodynamics can be misleading. The presence 2641  
 2641 of gravity means that it is impossible to have an isolated 2642  
 2642 system. To be convincing any proof of the second law 2643  
 2643 of thermodynamics should include the universe and its 2644  
 2644 gravitational interactions in the proof. 2645

4.21. Olber's Paradox

2646 For Curvature-cosmology, Olber's Paradox is not a 2647  
 2647 problem. Curvature-redshift is sufficient to move dis- 2648  
 2648 tant starlight out of the visible band. Visible light from 2649  
 2649 distant galaxies is shifted into the infrared where it is no 2650  
 2650 longer seen. Of course, with a finite universe, there is the 2651  
 2651 problem of conservation of energy and why we are not 2652  
 2652 saturated with very low frequency radiation produced by 2653  
 2653 Curvature-redshift. These low-energy photons are even- 2654  
 2654 tually absorbed by the cosmic plasma. Everything is re- 2655  
 2655 cycled. The plasma radiates energy into the microwave 2656  
 2656 background radiation and into X-rays. The galaxies de- 2657  
 2657 velop from the cosmic plasma and pass through their 2658  
 2658 normal evolution. Eventually all their material is re- 2659  
 2659 turned to the cosmic plasma. Note that very little, if 2660  
 2660 any, is locked up into black holes. Curvature-pressure 2661



causes most of the material from highly compact objects to be returned to the surrounding region as jets.

#### 4.22. Philip's relation

Phillips (1993) Showed that there was a good correlation between the peak magnitude and the width of the light curve for Type Ia supernova. For the Philip's relation to be meaningful, it must be between the absolute magnitude and the width corrected for its  $(1+z)$  dependence.

The slope of the regression of the absolute magnitudes (using the  $\Lambda$ CDM model and the intrinsic analysis) of Type Ia supernova for all the supernova versus the widths divided by  $(1+z)$  is  $(-0.009 \pm 0.091)$ . Which shows that for these observations of Type I a supernova there is no significant Phillip's relation which implies that SALT2 estimates of this relation may be an artifact of the SALT2 analysis.

### 5. CONCLUSIONS

This paper describes the Curvature-cosmology paradigm that challenges the big bang paradigm to see which provides the best agreement with cosmological observations. Following the precepts of Thomas S. Kuhn (Kuhn 1970) it is essential that each paradigm must be judged using its own analysis. That is observations of non-static behavior observed within the old paradigm cannot be used to invalidate the new paradigm. They must be evaluated within the new paradigm to have any validity.

The major support for the  $\Lambda$ CDM model is that it describes the general relativity model of an unstable expanding universe. This is similar to assuming that a falling feather should have the same acceleration as a falling stone, whereas we know that the difference is due to air resistance. Maybe cosmology needs something like air resistance such as Curvature-cosmology,

Crucially the standard procedure is to use  $\Lambda$ CDM or one of its variants to determine the dimensionless density parameters, which depend on assumptions of inflation, dark matter and dark energy. Since none of these properties are substantiated by other independent observations, they do not provide any support for this cosmology. Moreover they are ad hoc models largely determined by supernova observations. In other words, there are no observations other than those for supernova that show strong confirmation of the SALT2 analysis and the  $\Lambda$ CDM model.

Curvature-cosmology is a static tired-light cosmology which is a static solution to the equation of general relativity that is described by the Friedmann equations with an additional term that stabilizes the solution.

This term called Curvature-pressure is a reaction of high-speed particles back on the material producing the curved space-time. This sense of this reaction is to try and reduce the curvature.

The basic cosmological model is one in which the cosmic plasma dominates the mass distribution and hence the curvature of space-time. In this first-order model, the gravitational effects of stars and galaxies are neglected. The geometry C is that of a three-dimensional "surface" of a four-dimensional hyper-sphere, which is common to most cosmologies. Its main strengths are that it does not have ad hoc additions to the model and it has exceptionally good agreement with cosmological observations.

This is a brief summary of the quantitative observations that are relevant to the Curvature-cosmology model. The predicted Hubble's constant is

$$H_0 = c/R \text{ s}^{-1} \quad (54)$$

$$\begin{aligned} &= 2.364 \times 10^{-5} \sqrt{\rho} \text{ s}^{-1} \\ &= 9.6352 \times 10^{-19} \sqrt{N_\epsilon} \text{ s}^{-1} \\ &= 29.73 \sqrt{N_\epsilon} \text{ kms}^{-1} \text{ Mpc}^{-1} \\ &= 41.30 \text{ kms}^{-1} \text{ Mpc}^{-1}, \end{aligned} \quad (55)$$

where the last line has used  $N_\epsilon = 1.93$  from section 4.2. This value is significantly less than the current value of  $H_0 \approx 0.70$ . However these measurements were based the standard model. A valid test would be re-evaluate the observations using Curvature-cosmology.

For the 1,652 Type Ia supernova analyzed in Part A the light curve width is

$$w_{obs}(z) = 1.060 \pm 0.009 + (1.080 \pm 0.042) z,$$

and the regression of the absolute magnitudes as a function of redshift is

$$M(z) = -17.597 \pm 0.012 + (0.143 \pm 0.057) z,$$

Both results shows very strong support for Curvature-cosmology and can only be made consistent with  $\Lambda$ CDM by introducing dark energy.

It has been shown that the X-ray data in the range from about 10 Kev to about 300 kev can be explained by bremsstrahlung from the cosmic plasma. The fitted temperature was  $2.62 \pm 0.13 \times 10^9$  K, whereas the predicted temperature is  $2.46 \pm 0.04 \times 10^9$  K, which shows excellent agreement. The fitted density for the cosmic plasma is  $N_\epsilon = 1.93 \pm 0.04$  hydrogen atoms per  $\text{m}^3$  which is the only free parameter.

For Cosmic Microwave Background Radiation Curvature-cosmology predicts a temperature of 2.736 which is compared with the observed temperature of  $2.72548 \pm 0.00057$  K. There is excellent agreement.

2744 The standard cosmology predicts that the distribution  
2745 of Tolman surface brightness should have an exponent  
2746 of four, whereas Curvature-cosmology predicts an expo-  
2747 nent of one. The result is  $n = 1.38 \pm 0.13$  which is in  
2748 agreement with unity.

2749 Curvature-cosmology does not need dark matter to  
2750 explain the velocity dispersion in clusters of galaxies or  
2751 the shape of galactic rotation curves. Nor does it need  
2752 dark energy to explain type 1a supernova observations.  
2753 Furthermore it is shown in section 2.5 that dark energy  
2754 could be due to fault in the SALT2 analysis.

2755 For angular size the conclusion is in favor of  
2756 Curvature-cosmology.

2757 An analysis of many galaxies that have multiple ob-  
2758 served bands show no evidence of evolution.

2759 Curvature-cosmology predicts the observed quasar  
2760 epoch variability of zero.

2761 The Butcher-Oemler effect remains uncertain, and  
2762 therefore does not provide evidence to refute a static  
2763 cosmology.

2764 Fluctuations in the CMBR can be explained a density  
2765 fluctuations in the cosmic plasma.

2766 Not only can Curvature-cosmology explain the anomalous  
2767 Pioneer 10 acceleration, it has a feasible prediction  
2768 of its value.

2769 Overall for Curvature-cosmology there is remark-  
2770 able agreement between its predictions and observations,  
2771 without any serious problems.

## 2772 6. AUTHOR BIOGRAPHY

2773 David F. Crawford was born at Griffith, NSW, Aus-  
2774 tralia in 1937. He graduated BSc and PhD from School

2775 of Physics, University of Sydney. Half of his PhD thesis  
2776 was on designing and building a Geiger counter array  
2777 to study cosmic ray air-showers and the second half on  
2778 programming a three-dimensional Monte Carlo simula-  
2779 tion on the computer Silliac to calculate the energy and  
2780 structure of electron-photon cascades. The results pub-  
2781 lished in a 1,512-page book "Electron-photon Shower  
2782 Distribution Function" by H. Messel and D.F. Craw-  
2783 ford, Pergamon Press, 1970.

2784 He worked for two years from 1966 at Cornell Uni-  
2785 versity learning radar Astronomy. From 1969 to his re-  
2786 tirement in 2003, He provided computer analysis of ob-  
2787 servations from the Molonglo Radio Telescope. He is a  
2788 member of the Australian Astronomical Society. He has  
2789 been an author in 33 papers published in refereed jour-  
2790 nals. Since he wrote his first program in 1959, He has  
2791 had a major interest in computers and programming es-  
2792 pecially in the use of computers to analyze observations  
2793 and apply them to astrophysical theories. He also have  
2794 a long-time interest in the foundations of cosmology.

## 2795 ACKNOWLEDGMENTS

2796 This research has made use of the NASA/IPAC Ex-  
2797 tragalactic Database (NED) that is operated by the  
2798 Jet Propulsion Laboratory, California Institute of Tech-  
2799 nology, under contract with the National Aeronautics  
2800 and Space Administration. The calculations have used  
2801 Ubuntu Linux and the graphics have used the DISLIN  
2802 plotting library provided by the Max-Planck-Institute in  
2803 Lindau.

## REFERENCES

- 2804 Allen, C. W. 1976, *Astrophysical Quantities*  
2805 Amanullah, R., Lidman, C., Rubin, D., et al. 2010, *The*  
2806 *Astrophysical Journal*, 716, 712,  
2807 doi: [10.1088/0004-637X/716/1/712](https://doi.org/10.1088/0004-637X/716/1/712)  
2808 Anderson, J. D., Laing, P. A., Lau, E. L., et al. 2002,  
2809 *PhRvD*, 65, 082004, doi: [10.1103/PhysRevD.65.082004](https://doi.org/10.1103/PhysRevD.65.082004)  
2810 Andreon, S., Lobo, C., & Iovino, A. 2004, *MNRAS*, 349,  
2811 889, doi: [10.1111/j.1365-2966.2004.07554.x](https://doi.org/10.1111/j.1365-2966.2004.07554.x)  
2812 Arp, H. 1987, *Quasars, redshifts, and controversies*  
2813 —. 1992, *Monthly Notices of the Royal Astronomical*  
2814 *Society*, 258, 800, doi: [10.1093/mnras/258.4.800](https://doi.org/10.1093/mnras/258.4.800)  
2815 Beijersbergen, M. 2003, PhD thesis, University of  
2816 Groningen, Netherlands  
2817 Betoule, M., Kessler, R., Guy, J., et al. 2014, *Astronomy*  
2818 *and Astrophysics*, 568, A22,  
2819 doi: [10.1051/0004-6361/201423413](https://doi.org/10.1051/0004-6361/201423413)  
2820 Bielby, R. M., & Shanks, T. 2007, *Monthly Notices of the*  
2821 *Royal Astronomical Society*, 382, 1196,  
2822 doi: [10.1111/j.1365-2966.2007.12456.x](https://doi.org/10.1111/j.1365-2966.2007.12456.x)  
2823 Blanton, M. R., & Moustakas, J. 2009, *Annual Review of*  
2824 *Astronomy and Astrophysics*, 47, 159,  
2825 doi: [10.1146/annurev-astro-082708-101734](https://doi.org/10.1146/annurev-astro-082708-101734)  
2826 Blondin, S., Davis, T. M., Krisciunas, K., et al. 2008, *The*  
2827 *Astrophysical Journal*, 682, 724, doi: [10.1086/589568](https://doi.org/10.1086/589568)  
2828 Born, M., & Wolf, E. 1999, *Principles of Optics*  
2829 Braginskij, V. B., & Panov, V. I. 1971, *Uspekhi*  
2830 *Fizicheskikh Nauk*, 105, 779  
2831 Briel, U. G., Henry, J. P., & Boehringer, H. 1992, *A&A*,  
2832 259, L31  
2833 Buchalter, A., Helfand, D. J., Becker, R. H., & White,  
2834 R. L. 1998, *The Astrophysical Journal*, 494, 503,  
2835 doi: [10.1086/305236](https://doi.org/10.1086/305236)

- 2836 Butcher, H., & Oemler, A., J. 1978, *The Astrophysical*  
2837 *Journal*, 219, 18, doi: [10.1086/155751](https://doi.org/10.1086/155751)
- 2838 —. 1984, *The Astrophysical Journal*, 285, 426,  
2839 doi: [10.1086/162519](https://doi.org/10.1086/162519)
- 2840 Cabré, A., Gaztañaga, E., Manera, M., Fosalba, P., &  
2841 Castander, F. 2006, *Monthly Notices of the Royal*  
2842 *Astronomical Society*, 372, L23,  
2843 doi: [10.1111/j.1745-3933.2006.00218.x](https://doi.org/10.1111/j.1745-3933.2006.00218.x)
- 2844 Carlip, S. 1998, *American Journal of Physics*, 66, 409,  
2845 doi: [10.1119/1.18885](https://doi.org/10.1119/1.18885)
- 2846 Cassinelli, J. P. 1979, *Annual Review of Astronomy and*  
2847 *Astrophysics*, 17, 275,  
2848 doi: [10.1146/annurev.aa.17.090179.001423](https://doi.org/10.1146/annurev.aa.17.090179.001423)
- 2849 Chu, Y., Wei, J., Hu, J., Zhu, X., & Arp, H. 1998, *The*  
2850 *Astrophysical Journal*, 500, 596, doi: [10.1086/305779](https://doi.org/10.1086/305779)
- 2851 Colless, M., & Dunn, A. M. 1996, *ApJ*, 458, 435,  
2852 doi: [10.1086/176827](https://doi.org/10.1086/176827)
- 2853 Conley, A., Guy, J., Sullivan, M., et al. 2011, *The*  
2854 *Astrophysics Journal Supplement Series*, 192, 1,  
2855 doi: [10.1088/0067-0049/192/1/1](https://doi.org/10.1088/0067-0049/192/1/1)
- 2856 Cowsik, R., & Kobetich, E. J. 1972, *The Astrophysical*  
2857 *Journal*, 177, 585, doi: [10.1086/151735](https://doi.org/10.1086/151735)
- 2858 Crawford, D. F. 1987a, *Australian Journal of Physics*, 40,  
2859 459, doi: [10.1071/PH870459](https://doi.org/10.1071/PH870459)
- 2860 —. 1987b, *Australian Journal of Physics*, 40, 449,  
2861 doi: [10.1071/PH870449](https://doi.org/10.1071/PH870449)
- 2862 —. 1991, *ApJ*, 377, 1, doi: [10.1086/170330](https://doi.org/10.1086/170330)
- 2863 —. 1993, *ApJ*, 410, 488, doi: [10.1086/172765](https://doi.org/10.1086/172765)
- 2864 —. 1995a, *ApJ*, 440, 466, doi: [10.1086/175288](https://doi.org/10.1086/175288)
- 2865 —. 1995b, *ApJ*, 441, 488, doi: [10.1086/175375](https://doi.org/10.1086/175375)
- 2866 —. 1998, arXiv e-prints, astro.  
2867 <https://arxiv.org/abs/astro-ph/9803009>
- 2868 —. 1999a, *Australian Journal of Physics*, 52, 753,  
2869 doi: [10.1071/PH98065](https://doi.org/10.1071/PH98065)
- 2870 —. 1999b, arXiv e-prints, astro.  
2871 <https://arxiv.org/abs/astro-ph/9904150>
- 2872 —. 2006, *Curvature Cosmology*
- 2873 —. 2009a, arXiv e-prints, arXiv:0901.4169.  
2874 <https://arxiv.org/abs/0901.4169>
- 2875 —. 2009b, arXiv e-prints, arXiv:0901.4172.  
2876 <https://arxiv.org/abs/0901.4172>
- 2877 de Lapparent, V., Geller, M. J., & Huchra, J. P. 1986,  
2878 *ApJL*, 302, L1, doi: [10.1086/184625](https://doi.org/10.1086/184625)
- 2879 Dennis, B. R., Suri, A. N., & Frost, K. J. 1973, *The*  
2880 *Astrophysical Journal*, 186, 97, doi: [10.1086/152480](https://doi.org/10.1086/152480)
- 2881 Dicke, R. H. 1964, *Nature*, 202, 432, doi: [10.1038/202432a0](https://doi.org/10.1038/202432a0)
- 2882 Disney, M. J. 2000, *General Relativity and Gravitation*, 32,  
2883 1125, doi: [10.1023/A:1001981929727](https://doi.org/10.1023/A:1001981929727)
- 2884 Djorgovski, S., & Spinrad, H. 1981, *The Astrophysical*  
2885 *Journal*, 251, 417, doi: [10.1086/159478](https://doi.org/10.1086/159478)
- 2886 Ellis, G. F. R. 1984, *Annual Review of Astronomy and*  
2887 *Astrophysics*, 22, 157,  
2888 doi: [10.1146/annurev.aa.22.090184.001105](https://doi.org/10.1146/annurev.aa.22.090184.001105)
- 2889 Eötvös, R. V., Pekár, D., & Fekete, E. 1922, *Annalen der*  
2890 *Physik*, 373, 11, doi: [10.1002/andp.19223730903](https://doi.org/10.1002/andp.19223730903)
- 2891 Feynman, R. P. 1965, *Feynman lectures on physics*. Volume  
2892 3: Quantum mechanics
- 2893 Field, G. B., & Henry, R. C. 1964, *The Astrophysical*  
2894 *Journal*, 140, 1002, doi: [10.1086/148000](https://doi.org/10.1086/148000)
- 2895 Finoguenov, A., Briel, U. G., Henry, J. P., et al. 2004,  
2896 *Astronomy and Astrophysics*, 419, 47,  
2897 doi: [10.1051/0004-6361:20035765](https://doi.org/10.1051/0004-6361:20035765)
- 2898 Fixsen, D. J. 2009, *ApJ*, 707, 916,  
2899 doi: [10.1088/0004-637X/707/2/916](https://doi.org/10.1088/0004-637X/707/2/916)
- 2900 Fixsen, D. J., Cheng, E. S., Gales, J. M., et al. 1996, *The*  
2901 *Astrophysical Journal*, 473, 576, doi: [10.1086/178173](https://doi.org/10.1086/178173)
- 2902 Freedman, W. L., Madore, B. F., Gibson, B. K., et al. 2001,  
2903 *The Astrophysical Journal*, 553, 47, doi: [10.1086/320638](https://doi.org/10.1086/320638)
- 2904 Fukada, Y., Hayakawa, S., Ikeda, M., et al. 1975,  
2905 *Astrophysics and Space Science*, 32, L1,  
2906 doi: [10.1007/BF00646232](https://doi.org/10.1007/BF00646232)
- 2907 Giacconi, R., Gursky, H., Paolini, F. R., & Rossi, B. B.  
2908 1962, *Physics Review Letters*, 9, 439,  
2909 doi: [10.1103/PhysRevLett.9.439](https://doi.org/10.1103/PhysRevLett.9.439)
- 2910 Goldhaber, G., Boyle, B., Bunclark, P., et al. 1996, *Nuclear*  
2911 *Physics B Proceedings Supplements*, Vol. 51, 51, 123,  
2912 doi: [10.1016/S0920-5632\(96\)00493-8](https://doi.org/10.1016/S0920-5632(96)00493-8)
- 2913 Goldhaber, G., Groom, D. E., Kim, A., et al. 2001, *The*  
2914 *Astrophysical Journal*, 558, 359, doi: [10.1086/322460](https://doi.org/10.1086/322460)
- 2915 Gould, R. J., & Burbidge, G. R. 1963, *The Astrophysical*  
2916 *Journal*, 138, 969, doi: [10.1086/147698](https://doi.org/10.1086/147698)
- 2917 Gruber, D. E., Matteson, J. L., Peterson, L. E., & Jung,  
2918 G. V. 1999, *The Astrophysical Journal*, 520, 124,  
2919 doi: [10.1086/307450](https://doi.org/10.1086/307450)
- 2920 Grun, E., Kruger, H., Srama, R., et al. 1999, in  
2921 *AAS/Division for Planetary Sciences Meeting Abstracts*  
2922 *#31, AAS/Division for Planetary Sciences Meeting*  
2923 *Abstracts*, 55.03
- 2924 Grun, E., Zook, H. A., Fechtig, H., & Giese, R. H. 1985,  
2925 *Icarus*, 62, 244, doi: [10.1016/0019-1035\(85\)90121-6](https://doi.org/10.1016/0019-1035(85)90121-6)
- 2926 Gurvits, L. I., Kellermann, K. I., & Frey, S. 1999,  
2927 *Astronomy and Astrophysics*, 342, 378.  
2928 <https://arxiv.org/abs/astro-ph/9812018>
- 2929 Guy, J., Astier, P., Baumont, S., et al. 2007, *Astronomy*  
2930 *and Astrophysics*, 466, 11,  
2931 doi: [10.1051/0004-6361:20066930](https://doi.org/10.1051/0004-6361:20066930)
- 2932 Guy, J., Sullivan, M., Conley, A., et al. 2010, *Astronomy*  
2933 *and Astrophysics*, 523, A7,  
2934 doi: [10.1051/0004-6361/201014468](https://doi.org/10.1051/0004-6361/201014468)

- 2935 Havas, P. 1966, *American Journal of Physics*, 34, 753,  
2936 doi: [10.1119/1.1973468](https://doi.org/10.1119/1.1973468)
- 2937 Hawkins, M. R. S. 2003, *MNRAS*, 344, 492,  
2938 doi: [10.1046/j.1365-8711.2003.06828.x](https://doi.org/10.1046/j.1365-8711.2003.06828.x)
- 2939 —. 2010, *MNRAS*, 405, 1940,  
2940 doi: [10.1111/j.1365-2966.2010.16581.x](https://doi.org/10.1111/j.1365-2966.2010.16581.x)
- 2941 Holt, S. S. 1992, *Annals of the New York Academy of*  
2942 *Sciences*, 655, 263,  
2943 doi: [10.1111/j.1749-6632.1992.tb17076.x](https://doi.org/10.1111/j.1749-6632.1992.tb17076.x)
- 2944 Hoyle, F. 1962, *Astronomy*.
- 2945 Hoyle, F., Burbidge, G., Narlikar, J. V., & Livio, M. 2000,  
2946 *Physics Today*, 53, 71, doi: [10.1063/1.1341928](https://doi.org/10.1063/1.1341928)
- 2947 Hughes, J. P. 1989, *The Astrophysical Journal*, 337, 21,  
2948 doi: [10.1086/167084](https://doi.org/10.1086/167084)
- 2949 Itoh, N., Sakamoto, T., Kusano, S., Nozawa, S., &  
2950 Kohyama, Y. 2000, *The Astrophysical Journal*  
2951 *Supplement Series*, 128, 125, doi: [10.1086/313375](https://doi.org/10.1086/313375)
- 2952 Jackson, J. D. 1975, *Classical electrodynamics*
- 2953 Jones, D., Scolnic, D., Riess, A., et al. 2018, in *American*  
2954 *Astronomical Society Meeting Abstracts #231*, Vol. 231,  
2955 308.06
- 2956 Jones, D. O., Rodney, S. A., Riess, A. G., et al. 2013, *The*  
2957 *Astrophysical Journal*, 768, 166,  
2958 doi: [10.1088/0004-637X/768/2/166](https://doi.org/10.1088/0004-637X/768/2/166)
- 2959 Joseph, R. 2010, *Journal of Cosmology*, 6, 1547
- 2960 Kaiser, N., Burgett, W., Chambers, K., et al. 2010, in  
2961 *Ground-based and Airborne Telescopes III*, Vol. 7733,  
2962 77330E, doi: [10.1117/12.859188](https://doi.org/10.1117/12.859188)
- 2963 Karoji, H., Nottale, L., & Vigier, J. P. 1976, *Astrophysics*  
2964 *and Space Science*, 44, 229, doi: [10.1007/BF00650484](https://doi.org/10.1007/BF00650484)
- 2965 Kessler, R., Becker, A. C., Cinabro, D., et al. 2009a, *The*  
2966 *Astrophysical Journal Supplement Series*, 185, 32,  
2967 doi: [10.1088/0067-0049/185/1/32](https://doi.org/10.1088/0067-0049/185/1/32)
- 2968 Kessler, R., Bernstein, J. P., Cinabro, D., et al. 2009b,  
2969 *Publications of the Astronomical Society of the Pacific*,  
2970 121, 1028, doi: [10.1086/605984](https://doi.org/10.1086/605984)
- 2971 Kinzer, R. L., Jung, G. V., Gruber, D. E., et al. 1997, *The*  
2972 *Astrophysical Journal*, 475, 361, doi: [10.1086/303507](https://doi.org/10.1086/303507)
- 2973 Kormendy, J. 1977, *The Astrophysical Journal*, 218, 333,  
2974 doi: [10.1086/155687](https://doi.org/10.1086/155687)
- 2975 Kowalski, M., Rubin, D., Aldering, G., et al. 2008, *The*  
2976 *Astrophysical Journal*, 686, 749, doi: [10.1086/589937](https://doi.org/10.1086/589937)
- 2977 Kuhn, T. S. 1970, *The structure of scientific revolutions*
- 2978 Lal, A. K. 2010, *Journal of Cosmology*, 6, 1533
- 2979 Le Sergeant D'Hendecourt, L. B., & Lamy, P. L. 1980,  
2980 *Icarus*, 43, 350, doi: [10.1016/0019-1035\(80\)90180-3](https://doi.org/10.1016/0019-1035(80)90180-3)
- 2981 Lerner, E. J. 1991, *The big bang never happened*
- 2982 Lieu, R., Mittaz, J. P. D., & Zhang, S.-N. 2006, *The*  
2983 *Astrophysical Journal*, 648, 176, doi: [10.1086/505627](https://doi.org/10.1086/505627)
- 2984 Liu, M. C., & Graham, J. R. 2001, *The Astrophysical*  
2985 *Journal*, 557, L31, doi: [10.1086/323174](https://doi.org/10.1086/323174)
- 2986 Longair, M. S. 1991, *Astronomy*, 19, 95
- 2987 López-Corredoira, M. 2010, *International Journal of*  
2988 *Modern Physics D*, 19, 245,  
2989 doi: [10.1142/S0218271810016397](https://doi.org/10.1142/S0218271810016397)
- 2990 Lubin, L. M., & Sandage, A. 2001a, *The Astronomical*  
2991 *Journal*, 121, 2289, doi: [10.1086/320401](https://doi.org/10.1086/320401)
- 2992 —. 2001b, *The Astronomical Journal*, 122, 1071,  
2993 doi: [10.1086/322133](https://doi.org/10.1086/322133)
- 2994 —. 2001c, *The Astronomical Journal*, 122, 1084,  
2995 doi: [10.1086/322134](https://doi.org/10.1086/322134)
- 2996 Lyke, B. W., Higley, A. N., McLane, J. N., et al. 2020, *The*  
2997 *Astrophysical Journal Supplement Series*, 250, 8,  
2998 doi: [10.3847/1538-4365/aba623](https://doi.org/10.3847/1538-4365/aba623)
- 2999 Mandrou, P., Vedrenne, G., & Niel, M. 1979, *The*  
3000 *Astrophysical Journal*, 230, 97, doi: [10.1086/157065](https://doi.org/10.1086/157065)
- 3001 Marshall, F. E., Boldt, E. A., Holt, S. S., et al. 1980, *The*  
3002 *Astrophysical Journal*, 235, 4, doi: [10.1086/157601](https://doi.org/10.1086/157601)
- 3003 Mather, J. C., Cheng, E. S., Eplee, R. E., J., et al. 1990,  
3004 *The Astrophysical Journal*, 354, L37, doi: [10.1086/185717](https://doi.org/10.1086/185717)
- 3005 Mayall, N. U. 1960, *Annales d'Astrophysique*, 23, 344
- 3006 Mazets, E. P., Golenetskii, S. V., Ilinskii, V. N., Gurian,  
3007 I. A., & Kharitonova, T. V. 1975, *Astrophysics and Space*  
3008 *Science*, 33, 347, doi: [10.1007/BF00640104](https://doi.org/10.1007/BF00640104)
- 3009 Misner, C. W., Thorne, K. S., & Wheeler, J. A. 1973,  
3010 *Gravitation*
- 3011 Nottale, L. 1976, *The Astrophysical Journal*, 208, L103,  
3012 doi: [10.1086/182242](https://doi.org/10.1086/182242)
- 3013 Nottale, L., & Vigier, J. P. 1977, *Nature*, 268, 608,  
3014 doi: [10.1038/268608a0](https://doi.org/10.1038/268608a0)
- 3015 Nozawa, S., Itoh, N., & Kohyama, Y. 1998, *The*  
3016 *Astrophysical Journal*, 507, 530, doi: [10.1086/306352](https://doi.org/10.1086/306352)
- 3017 Peebles, P. J. E. 1993, *Principles of Physical Cosmology*
- 3018 Petrosian, V. 1976, *The Astrophysical Journal*, 210, L53,  
3019 doi: [10.1086/182301](https://doi.org/10.1086/182301)
- 3020 Pettini, M., Hunstead, R. W., Smith, L. J., & Mar, D. P.  
3021 1990, *Monthly Notices of the Royal Astronomical*  
3022 *Society*, 246, 545
- 3023 Phillips, M. M. 1993, *The Astrophysical Journal Letters*,  
3024 413, L105, doi: [10.1086/186970](https://doi.org/10.1086/186970)
- 3025 Pimblet, K. A. 2003, *Publications of the Astronomical*  
3026 *Society of Australia*, 20, 294, doi: [10.1071/AS03043](https://doi.org/10.1071/AS03043)
- 3027 Postman, M., & Lauer, T. R. 1995, *The Astrophysical*  
3028 *Journal*, 440, 28, doi: [10.1086/175245](https://doi.org/10.1086/175245)
- 3029 Pound, R. V., & Snider, J. L. 1965, *Physical Review*, 140,  
3030 788, doi: [10.1103/PhysRev.140.B788](https://doi.org/10.1103/PhysRev.140.B788)
- 3031 Ratcliffe, H. 2010, *Journal of Cosmology*, 4, 693



- 3032 Rauch, M. 1998, *Annual Review of Astronomy and*  
3033 *Astrophysics*, 36, 267,  
3034 doi: [10.1146/annurev.astro.36.1.267](https://doi.org/10.1146/annurev.astro.36.1.267)
- 3035 Raychaudhuri, A. 1955, *Physical Review*, 98, 1123,  
3036 doi: [10.1103/PhysRev.98.1123](https://doi.org/10.1103/PhysRev.98.1123)
- 3037 Riess, A. G., Strolger, L.-G., Casertano, S., et al. 2007, *The*  
3038 *Astrophysical Journal*, 659, 98, doi: [10.1086/510378](https://doi.org/10.1086/510378)
- 3039 Rood, H. J. 1988, *Annual Review of Astronomy and*  
3040 *Astrophysics*, 26, 245,  
3041 doi: [10.1146/annurev.aa.26.090188.001333](https://doi.org/10.1146/annurev.aa.26.090188.001333)
- 3042 Rood, H. J., & Struble, M. F. 1982, *The Astrophysical*  
3043 *Journal*, 252, L7, doi: [10.1086/183708](https://doi.org/10.1086/183708)
- 3044 Roth, K. C., & Meyer, D. M. 1995, *The Astrophysical*  
3045 *Journal*, 441, 129, doi: [10.1086/175343](https://doi.org/10.1086/175343)
- 3046 Sandage, A. 2010, *The Astronomical Journal*, 139, 728,  
3047 doi: [10.1088/0004-6256/139/2/728](https://doi.org/10.1088/0004-6256/139/2/728)
- 3048 Sandage, A., & Lubin, L. M. 2001, *The Astronomical*  
3049 *Journal*, 121, 2271, doi: [10.1086/320394](https://doi.org/10.1086/320394)
- 3050 Sandage, A., & Perelmuter, J.-M. 1990, *The Astrophysical*  
3051 *Journal*, 361, 1, doi: [10.1086/169161](https://doi.org/10.1086/169161)
- 3052 Santangelo, N., Horstman, H., & Horstman-Moretti, E.  
3053 1973, *SoPh*, 29, 143, doi: [10.1007/BF00153445](https://doi.org/10.1007/BF00153445)
- 3054 Scolnic, D. M., Jones, D. O., Rest, A., et al. 2017, *ArXiv*  
3055 e-prints. <https://arxiv.org/abs/1710.00845>
- 3056 —. 2018, *The Astrophysical Journal*, 859, 101,  
3057 doi: [10.3847/1538-4357/aab9bb](https://doi.org/10.3847/1538-4357/aab9bb)
- 3058 Sunyaev, R. A., & Zeldovich, I. B. 1980, *Monthly Notices of*  
3059 *the Royal Astronomical Society*, 190, 413,  
3060 doi: [10.1093/mnras/190.3.413](https://doi.org/10.1093/mnras/190.3.413)
- 3061 Sunyaev, R. A., & Zeldovich, Y. B. 1970, *Astrophysics and*  
3062 *Space Science*, 9, 353, doi: [10.1007/BF00649576](https://doi.org/10.1007/BF00649576)
- 3063 Tolman, R. C. 1934, *Relativity, Thermodynamics, and*  
3064 *Cosmology*
- 3065 Trombka, J. I., Dyer, C. S., Evans, L. G., et al. 1977, *The*  
3066 *Astrophysical Journal*, 212, 925, doi: [10.1086/155117](https://doi.org/10.1086/155117)
- 3067 van Flandern, T. 1991, in *Bulletin of the American*  
3068 *Astronomical Society*, Vol. 23, 1395
- 3069 Watt, M. P., Ponman, T. J., Bertram, D., et al. 1992,  
3070 *Monthly Notices of the Royal Astronomical Society*, 258,  
3071 738, doi: [10.1093/mnras/258.4.738](https://doi.org/10.1093/mnras/258.4.738)
- 3072 White, S. D. M., Briel, U. G., & Henry, J. P. 1993,  
3073 *Monthly Notices of the Royal Astronomical Society*, 261,  
3074 L8, doi: [10.1093/mnras/261.1.L8](https://doi.org/10.1093/mnras/261.1.L8)
- 3075 Wolf, C., Wisotzki, L., Borch, A., et al. 2003, *Astromomy*  
3076 *and Astrophysics*, 408, 499,  
3077 doi: [10.1051/0004-6361:20030990](https://doi.org/10.1051/0004-6361:20030990)
- 3078 Wolf, C., Meisenheimer, K., Kleinheinrich, M., et al. 2004,  
3079 *Astromomy and Astrophysics*, 421, 913,  
3080 doi: [10.1051/0004-6361:20040525](https://doi.org/10.1051/0004-6361:20040525)
- 3081 Wood-Vasey, W. M., Friedman, A. S., Bloom, J. S., et al.  
3082 2008, *The Astrophysical Journal*, 689, 377,  
3083 doi: [10.1086/592374](https://doi.org/10.1086/592374)
- 3084 Zwicky, F. 1937, *The Astrophysical Journal*, 86, 217,  
3085 doi: [10.1086/143864](https://doi.org/10.1086/143864)